Science

Surface textures of Mars' north polar layered deposits: A framework for interpretation and future exploration

Sarah M. Milkovich[1,2] and James W. Head III[1]

[1]*Dept. of Geological Sciences, Box 1846, Brown University, Providence, RI, 02912, USA*
[2]*Now at Jet Propulsion Laboratory, Pasadena, CA, 91109, USA,* sarah.m.milkovich@jpl.nasa.gov

Abstract

Background: The deposition of layers within the north polar layered deposits (NPLD) is thought to be controlled by changing climate influencing the relative proportions of ice and dust accumulated in the polar regions; thus the NPLD are considered to contain the record of recent climate change on Mars and are important targets for future exploration. The physical properties and history of these layers remain relatively unknown. No detailed analysis of the morphology and texture of individual layer surfaces has been carried out until now; doing so can provide insight into the properties of the layers themselves and highlight useful measurements to make in the course of future exploration of the deposits and demonstrate what conditions such missions - especially rovers or drills - will face.

Approach: Of the 214 highest-resolution images available of the north polar region at the time of this study, 36 contain exposures of the NPLD. We examined the morphological characteristics of the surfaces of individual layers and compared them to those of terrestrial ice sheets in order to consider what physical characteristics may cause the morphologies observed in the NPLD, and to outline what future measurements will aid in understanding the processes that formed and shaped these deposits.

Results: The surfaces of the NPLD examined in the highest resolution images available display a variety of surface textures and resistances to erosion and erosion style. We classify layers according to their distinguishing characteristics; these classifications include knobby, pitted, rough, imbricated, and laminated layer textures. Several layers display evidence for deformation. Ten images between 4° and 40°E contain layer sequences that appear to include unconformities.

Interpretations: Mechanisms for forming these surface textures may include variations in erosion rates and styles of layers with different physical properties such as ice to dust ratio or ice grain size. We propose a conceptual model where variations in surface characteristics can be explained through climate influence on dust and ice deposition followed by subsequent erosion of this material. Potential angular unconformities and deformation features imply that portions of the NPLD have a complex history that may include periods of significant erosion as well as some amount of flow.

Conclusion: A comparison of terrestrial ice surfaces and martian layer bed surfaces provides insight into the history of polar processes. The textures of exposed individual layer surfaces may be heavily influenced by the physical properties of the underlying layer; such properties - and therefore the surface textures as well - may be influenced by climate variations. We propose a simple conceptual model in which layer surface texture is controlled by cyclical variation of dust content in the NPLD. We identify a number of observations that future polar surface missions should make to help distinguish among hypotheses. The diverse nature of these deposits indicate that ideally, future missions should be capable of analyzing the NPLD across multiple layers in multiple locations. Any mobile platform will need to be able to navigate rough surfaces as observed in many layers.

Introduction

Within the northern residual polar deposits of Mars are dark lanes or troughs; exposed on their walls are layered deposits that consist of extensive lateral layers of ice and dust found throughout the polar deposits (Figure 1). The upper layers, known as the north polar layered deposits (NPLD), were first identified in Mariner 9 images (e. g., Cutts 1973; Soderblom et al. 1973) and later studied in detail with the Viking orbiters (e.g., Kieffer et al. 1976; Blasius et al. 1982; Howard et al. 1982) and higher resolution Mars Global Surveyor (MGS) Mars Orbiter Camera (MOC) images (e.g., Malin and Edgett 2001; Kolb and Tanaka 2001; Laskar et al. 2002; Milkovich and Head 2005). Individual layers show considerable variation in thickness and resistance to erosion (Malin and Edgett 2001). Layers have been traced between neighboring troughs (Kolb and Tanaka 2001) and across at least three quarters of the northern deposits (Milkovich and Head 2005). Underneath the NPLD are the dark, platy layers of the Basal Unit (BU) (Kolb and Tanaka 2001; Byrne and Murray 2002; Edgett et al. 2003; Fishbaugh and Head, 2005). On the very surface of the NPLD is the residual water ice cap; the residual cap may be a separate deposit (e.g., Thomas et al. 1992) or may simply be the uppermost layer of the NPLD in the process of formation (e.g., Tanaka 2005).

Clifford et al. (2000) outlined four major questions driving research in polar science: 1) What is the composition, structure, and chronology expressed in the stratigraphy of the polar deposits? 2) What is their mass and energy budget, and what processes control them on seasonal and longer timescales? 3) What is their dynamical history? 4) Are there places within the polar regions where liquid water is or was present that may have provided habitats for past or present life?

There are a number of different lines of evidence about the components making up the polar deposits, their composition, and rheological behavior. In this paper, we highlight our current knowledge of these components of the martian north polar deposits as well as review the surface and interior characteristics of similar terrestrial ice and dust deposits in order to provide a framework for interpretation of polar deposits on Mars. We examine the highest-resolution images

available from MGS MOC to characterize the surface features visible at meters scale in the NPLD. Finally, we consider what the implications of these meters-scale features are for the questions outlined above as well as for directions of future research and exploration.

Mars North Polar Layered Deposits

Ice components

The NPLD are potentially made of water ice, solid CO_2, CO_2 clathrate hydrates ($CO_2 \cdot 6H_2O$) and dust in unknown proportions (e.g., Miller and Smythe 1970; Kieffer et al. 1976; Hofstadter and Murray 1990; Kargel and Lunine 1998; Hoffman 2000). Recent measurements by Mars Express' OMEGA visible-near-IR imaging spectrometer indicate that the surface is predominantly large-grained water ice (Langevin et al. 2005). Zuber et al. (1998) examined topographic data from the Mars Orbiter Laser Altimeter (MOLA) onboard MGS and concluded that CO_2 cannot be the main component of the NPLD; CO_2 is rheologically weak (Clark and Mullin 1976) and if the NPLD were primarily CO_2 they would deform under their own weight (Nye et al. 2000) and have a different planform than is observed.

Dust components

Figure 2 summarizes the sources for non-volatile material in the NPLD discussed in the next few sections. The thermal inertia of the NPLD is relatively high, indicating the presence of near-surface dust-contaminated ice (Paige et al. 1994) while the thermal inertia of the south polar layered deposits (SPLD) at the southern pole is extremely low, indicating the presence of a mantling material covering the SPLD (Paige and Keegan 1994). Hofstadter and Murray (1990) reported observing a lack of flow features in the polar layered deposits, concluding that the polar materials are not flowing and must therefore either have a dust content of over 60% or must consist of pure water ice. More recent laboratory experiments demonstrate that pure water ice could flow under present polar conditions (Durham et al. 1997). Recent OMEGA spectral measurements correspond to low concentrations (0 to 6% by volume) of dust contamination in
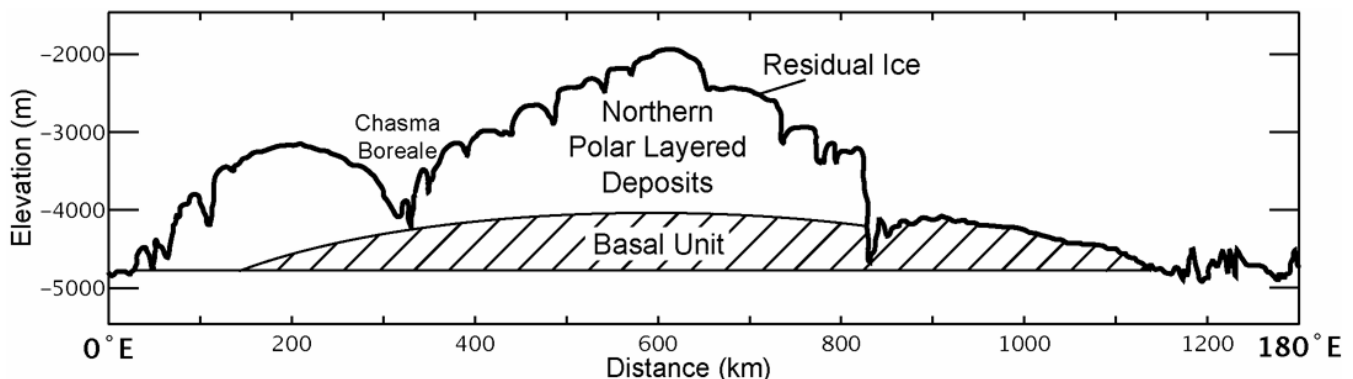

Figure 1. Cross section of the north polar deposits, made up of the Basal Unit (BU), the Northern Polar Layered Deposits (NPLD), and the residual ice cap, which may be the uppermost layer of the NPLD. After Byrne and Murray (2002) with modifications based on Fishbaugh and Head (2005). Topography is MOLA profile 11734 with a vertical exaggeration of 100.

the deposit surface; however, the exact amount of dust is model-dependent (Langevin et al. 2005). Initial subsurface sounding data from the Mars Advanced Radar for Subsurface and Ionospheric Sounding (MARSIS) onboard Mars Express indicates that the NPLD has a dielectric constant and loss tangent similar to "fairly pure water ice" (Picardi et al. 2005). Thus, the amount of dust in the deposits remains unknown but is likely small. The dust in both the NPLD and SPLD is similar in color and albedo for the most part to the ubiquitous dust that is found over the rest of the planet (e. g., Thomas and Weitz 1989; Herkenhoff and Murray 1990). Dunes and dust deposits are found around the polar deposits; dark dunes located on Olympia Planitia (~240°E) correspond to the location of calcium-rich sulfate (such as gypsum) deposits observed by OMEGA and imply that some minerals in the polar regions have been altered by water (Langevin et al. 2005).
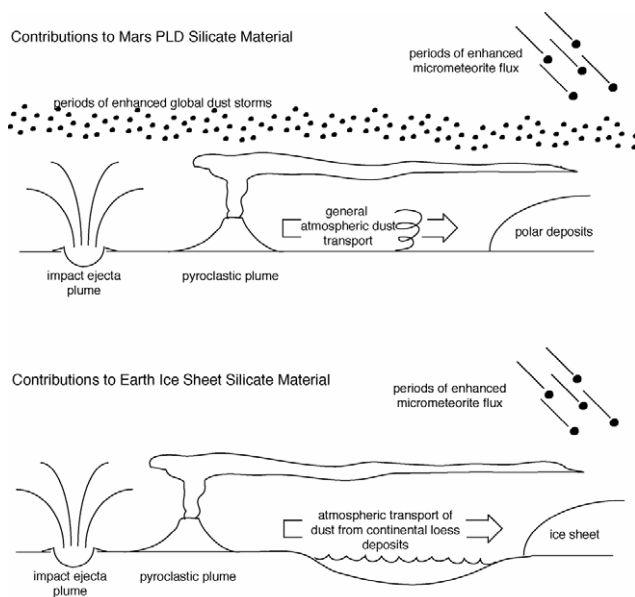

Figure 2. Sources for dust layers within ice deposits. Top: Sources for martian NPLD. Bottom: Sources for terrestrial ice sheets.

Dust layers are found in terrestrial ice cores around the world and are used to trace atmospheric circulation patterns in climate history studies (e.g., Petit et al. 1990; Bory et al. 2003; Kang et al. 2003). The chemical composition of an individual dust layer can provide information on source regions (Figure 2) (Bory et al. 2003; Kang et al. 2003). Dust layers within ice cores have been correlated with both marine sediments and continental loess deposits, and vary with Earth's orbital parameters (Petit et al. 1990). Layers can also record the stress conditions within ice sheets; layers at depth within flowing ice sheets become thinner through compaction from overburden and deform as the ice flows over the underlying topography. Layer deformation is discussed further in a later section.

Due to the large variations in Martian obliquity (e.g., Ward 1992; Laskar et al. 2004), zones of ice stability move from the poles to the equator and back over time (e.g. Jakosky et al. 1993; Mellon and Jakosky 1995; Levrard et al. 2004). When an ice stability zone moves, ice deposits within the zone sublimate and the ice moves to a new region. Dust layers contained within these icy deposits will be left behind and form dust lag deposits. Such deposits can form a protective surface layer, cutting off the underlying ice from the atmosphere and preventing any further sublimation. In this way, some amount of ice deposits from previous climate regimes can be preserved around the planet, including equatorial glacial deposits (Head and Marchant 2003).

Additional components

Darker material is also found in the polar regions and may represent volcanic ash or filamentary sublimate residue particles derived from erosion of the deposit (Herkenhoff and Vasavada 1999). Ejecta material such as microtektites from major or nearby impacts may also be found in the layered deposits (Lorenz 2000; Wrobel and Schultz 2004). Recent considerations of ejecta dispersal around a spherical planet indicate that oblique impacts may spread ejecta much further than previously thought and so contribute more material to airfall deposits (Schultz and Mustard 2001) such as the NPLD.

Volcanic material may also contribute to the NPLD; the surface of the NPLD has a crater retention age of ~100,000 years (Herkenhoff and Plaut 2000). While the surface age of the NPLD can be calculated by counting craters, the age of the internal layers is not easy to constrain. NPLD accumulation likely has been sporadic and dependent on orbital and axial positions with periods of no net accumulation during times of high obliquity (e.g., Milkovich et al. 2006; Milkovich and Head 2005; Head et al. 2003; Haberle et al. 2003; Jakosky et al. 1995). Directly below the NPLD is the Basal Unit, with a crater age of Middle to Late Amazonian, although it is difficult to date since very little surface area of the deposit is exposed (Fishbaugh and Head 2005). The NPLD may therefore have begun to form as early as the Middle Amazonian, many hundreds of Myrs ago. While the age and amount of the most recent episodes of volcanism on Mars are still under debate, near-polar landforms have been suggested to be volcanic structures formed 1-20 million years ago (Garvin et al. 2000), and lava flows elsewhere in the Elysium and Cerberus regions and volcanics in the Tharsis Montes may have formed in the last 10 million years (Hartmann and Berman 2000; Berman and Hartmann 2002, Marquez et al. 2004). Thus it is possible that Mars was volcanically active at some point during the formation of the NPLD, and volcanic products may be found in the NPLD.

Volcanic eruptions produce sulfate aerosol particles that would be globally distributed through atmospheric circulation (Settle 1979) which may contribute to the material in the layered deposits. Solid volcanic material may make its way to the NPLD as well. Tephra is a collective term for deposits of airborne solid fragments of volcanic material. Layers of tephra have been found within ice cores around the world, as well as in terrestrial and marine sediments. They have proven extremely useful for

correlating stratigraphic sequences between multiple locations due to the fact that a single tephra layer is essentially deposited simultaneously at all locations. They also provide a record of historical volcanic eruptions.

Due to the lower atmospheric pressure on Mars compared to the Earth, explosive eruptions should be common in martian history, eruption clouds should rise about 5 times higher for the same eruption rate, and deposits should be systematically finer grained by a factor of 100 than those on Earth (Wilson and Head 1994). Recent theoretical studies of explosive eruption products on Mars indicates that millimeter-scale particles may be formed and dispersed (Wilson and Head 2005). Particles produced by martian volcanic eruptions around the planet will be globally distributed through atmospheric circulation similar to the aerosols (Settle 1979). Thus, it is important to be able to recognize tephra layers within the NPLD.

Tephra includes a range of fragment sizes, divided into ash (<2 mm), lapilli (2-64 mm), and blocks or bombs (>64 mm), though the tephra found in ice cores are predominantly ash-sized due to the distances from volcanic sources (Haflidason et al. 2000). Individual tephra fragments found in Antarctica and Greenland ice range in diameter from 0.5 to 100 µm (Palais et al. 1988; Zielinski et al. 1997; Dunbar et al. 2003). The morphology of tephra is controlled by forces during the volcanic eruption including gas-driven expansion of fluid magma and cooling rates; tephra may also experience erosion, transport, and redeposition that may alter their morphology (Haflidason et al. 2000). The most common component of tephra is small, angular glass shards; many of the larger shards contain elongated pipe-shaped vesicles while the smaller particles include vesicular bubbles and non-vesicular blocks (Palais et al. 1988). Additional components of tephra are lithic fragments and crystalline particles. The finer tephra grains have little to no vesicularity and tend to be 1-2 µm in diameter. These fine ash particles tend to combine with glass shards and lithic fragments to form aggregates 5-50 µm in size (Palais et al. 1988).

Some tephra layers exhibit chemical alteration in thin coatings or rims on the outer surfaces of the individual particles; this alteration can be due to interactions with volatiles in the eruptive clouds before emplacement on the ice (Palais et al. 1988), or due to leaching of material from the tephra into the surrounding substrate (Pollard et al. 2003). This last mechanism is dependent on the chemical makeup of the individual tephra deposit and the nature of the substrate; for example, basaltic tephra are more chemically unstable in an aqueous environment than rhyolitic tephra (Pollard et al. 2003). Nevertheless, many tephra are chemically stable enough to be correlated with specific eruptions from individual volcanoes (Palais et al. 1988; Zielinski and Germani 1998; Haflidason et al. 2000; Dunbar et al. 2003).

Thicknesses of tephra layers vary with the proximity to the volcanic source and size of the eruption. Any tephra layers identified at the martian north pole may be extremely thin; terrestrial tephra layers are often on the order of 1-10 cm in

thickness when the volcanic eruption is hundreds of km away (Palais et al. 1988; Haflidason et al. 2000). A tephra layer, like an impact ejecta layer, will be independent of orbital-influenced climate cycles and may be useful for assigning ages to the polar stratigraphic record. The High Resolution Imaging Science Experiment (HiRISE) onboard Mars Reconnaissance Orbiter will be able to resolve a 10 cm thick tephra layer exposed on a shallow trough slope (~5°) if one exists; however as trough slopes can be steeper than 5° and any tephra layers present may be less than 10 cm thick, detection of tephra layers is better suited for surface exploration through a rover or a drill. Identification of a tephra layer can be based on the color and morphological characteristics (as described above) of the individual glass grains (Haflidason et al. 2000).
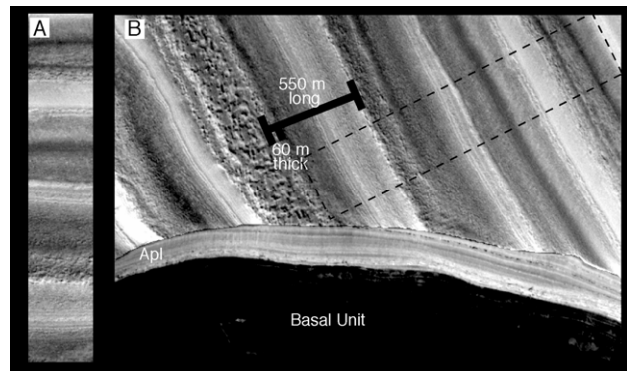

Figure 3. The effect of slope on layer exposure. A) Subframe of MOC image E02/01209. B) Larger subframe of MOC image E02/01209; this image has been contrast enhanced in two different ways and recompiled in order to bring out the details of layers on the cliff wall (middle) and the trough wall (left). The scale bar shows the horizontal distance along the surface between a pair of layers exposed on the trough wall on the left and the true thickness of the same layers as exposed on the cliff wall in the middle. The dark unit on the right is the basal unit underlying the NPLD and appears featureless due to the contrast enhancement. (figure3.png)

The NPLD are exposed on very shallow slopes; average trough slopes are less than 8°. It is important to realize that the appearance of individual layers in a specific image represents an apparent thickness, and is controlled by the slope of the exposed surface (e.g., trough wall). For example, Figure 3a contains a typical layer sequence. This sequence is taken from a larger image (location indicated by box in Figure 3b); a vertical view of a layered sequence or section is seen in the MOC image (upper section) and a particular 550 m long section is indicated by the dark bar. The 550 meters distance is the distance along the ground and is thus an apparent thickness. A 40° sloping cliff of this same stratigraphic section is also exposed in this image (Figure 3b, middle, labeled Apl) and it is clearly seen that the layers are generally planar and exposed along a very shallow slope (Figure 3b, upper section). The MOLA altimetry data then permit this slope to be measured and a true layer or unit thickness calculated. In this case, MOLA data show that the slope is ~6 degrees and that the actual thickness of the 550 m exposed section is ~60 m, about one tenth of the apparent

thickness in the image. In all figures of the NPLD, we use two scale bars: one indicates the scale in terms of actual surface distance calculated from the image resolution and the other indicates the equivalent height in a vertical column based on the MOLA topography data associated with each image (compare Figure 3 a and b).

Table 1. 36 highest-resolution MOC images used in texture analysis

Image Number	Center Latitude °N	Center Longitude °E	Resolution m/pxl
E19/00675	80.88	32.58	1.69
E22/01049	84.66	3.45	1.70
E22/01609	85.24	350.40	1.70
FHA/01474	83.97	266.66	1.60
FHA/01488	84.83	203.46	1.60
FHA/01515	83.30	98.31	1.60
FHA/01546	86.28	230.65	1.60
FHA/01596	82.15	90.02	1.60
FHA/01643	85.46	145.89	1.61
M00/00024	85.44	187.27	1.60
M00/00163	84.83	124.12	1.61
M00/01609	83.46	334.08	1.61
M00/01646	84.48	254.10	1.61
M00/01714	84.08	108.95	1.61
M00/01733	86.80	165.68	1.61
M00/01734	83.61	77.54	1.61
M00/01754	86.55	78.08	1.62
M00/02072	85.96	101.11	1.61
M00/02100	86.48	80.46	1.62
M00/02242	86.87	194.62	1.62
M00/02416	79.61	352.28	1.61
M00/02418	85.37	240.35	1.62
M00/02936	84.31	226.01	1.63
M01/00034	85.71	298.06	1.63
M01/00208	84.17	262.96	1.62
M02/00061	84.87	210.76	1.62
M02/00747	79.20	338.55	1.62
M02/02115	87.12	95.20	1.62
M02/02431	83.79	115.81	1.62
M02/02744	85.20	146.60	1.61
M02/04374	86.51	79.43	1.62
R01/00025	84.61	3.00	1.69
R01/00641	83.08	94.60	1.67
R01/01449	83.94	121.64	1.71
R03/00353	83.88	121.49	1.70

NPLD formation

While the details of the formation processes of the NPLD remain unknown, a general model has emerged based on Viking analyses (e.g., Squyres 1979; Cutts and Lewis 1982; Howard et al. 1982) and refined with analyses of MOC images (e.g., Malin and Edgett 2001; Kolb and Tanaka 2001; Laskar et al. 2002; Milkovich and Head 2005; Milkovich et al. 2006; Tanaka 2005; Fishbaugh and Hvidberg 2006) combined with climate models (e.g., Paige 1992; Jakosky et al. 1995; Mischna et al. 2003). Obliquity has traditionally been invoked to drive the variation between layers because it has a major effect on the insolation received at the polar regions, and insolation controls temperature and ice stability (e.g., Squyres 1979; Cutts and Lewis 1982; Howard et al. 1982). However, other orbital elements, including

eccentricity and longitude of perihelion, affect the distribution and intensity of insolation as well (e.g., Mischna et al. 2003). Quasi-periodic changes all these orbital elements cause rhythmic fluctuations in insolation and thus climate in a similar manner to the Milankovitch theory of ice ages on Earth (e. g., Hayes et al. 1976; Imbrie 1982). The changing climate affects the atmospheric pressure, regions of ice stability, and atmospheric dust loading through time. This in turn changes the dust-to-ice ratio of material accumulated in the polar regions. Thus, variations between layers in the NPLD record the recent fluctuations of the martian climate. Translating this record would provide valuable insights into the mechanics of climate change. While much has been learned from recent spacecraft images and topography data at a variety of scales, we are only beginning to be able to directly link sections of NPLD with specific periods of the climate record (Laskar et al. 2002; Milkovich and Head 2005; Milkovich et al. 2006). Milkovich and Head (2005) and Milkovich et al. (2006) have examined the polar layered deposits for climate signals using Fourier analysis; they identified a "no signal" zone ~300 meters below the deposit surface where such signals are absent and interpreted it as the lag deposit from the most recent migration of volatiles to the mid-latitudes due to a decrease in obliquity approximately 0.5 million years ago.

A complication in understanding the properties and composition of the NPLD is that all image and topographic analysis has been based on observations of the surface exposure of the NPLD. It is possible that surface-atmosphere interactions have resulted in a surface lag or alteration rind that is different than the underlying material. The true nature of the underlying NPLD material remains unknown.
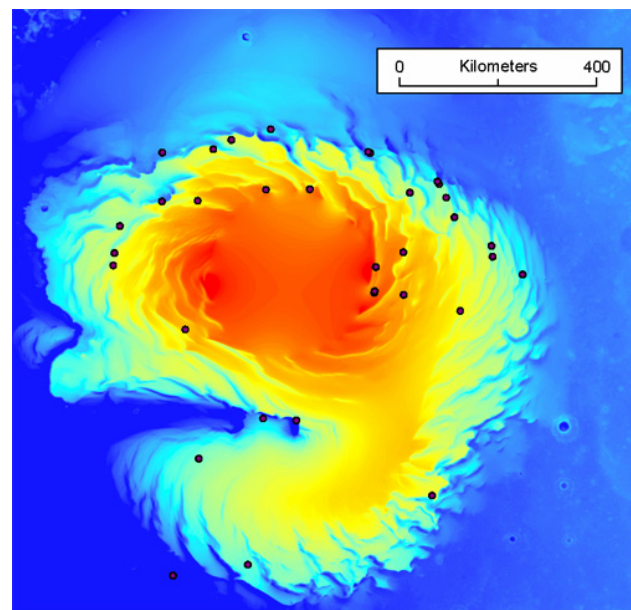

Figure 4. Locations of highest-resolution MOC images used in the texture analysis superimposed on the north polar deposit topography data.
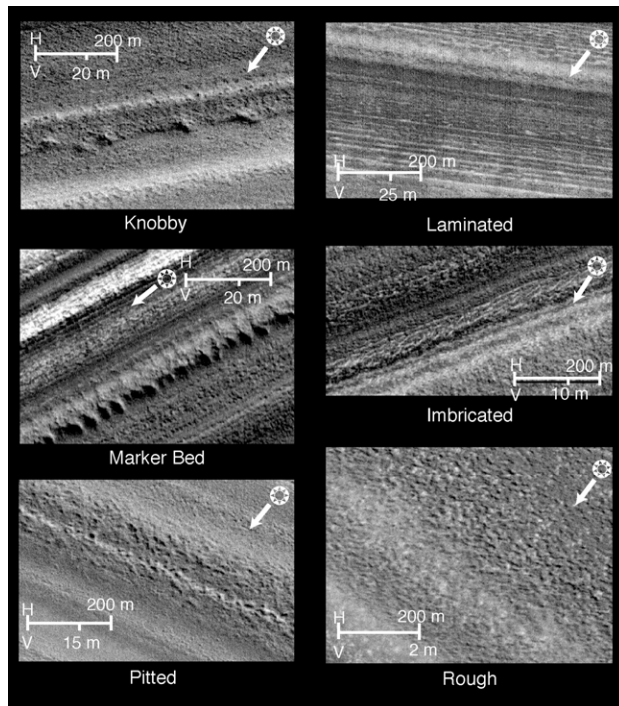
Figure 5. Surface textures in the NPLD. Counter clockwise from upper left: knobby (M00/00163), the marker bed (M00/02100), pitted (M02/02431), rough (M01/00034), imbricate (M01/01754), laminated (M02/00061). Sun direction indicated by arrows. Scale bar indicates the horizontal scale derived from the image on top and vertical scale derived from MOLA data on bottom (figure5.png).

NPLD Observations

Surface textures

The surface exposure of layers is likely to represent the combination of physical characteristics of the layer itself and post-depositional process such as volatile sublimation and erosion. An examination of the surfaces can provide clues to what processes are at work in the polar region that in turn will provide insight into the evolution and history of the NPLD. The highest resolution MOC images available (< 2.0 m/pxl) were examined in order to characterize individual layers in detail. Of the 214 images available of the polar region at this resolution at the time of analysis, 36 had clear exposures of the NPLD (Table 1, Figure 4).

A variety of surface textures can be seen in the thirty-six highest resolution images. They fall into five categories, which are described below. Figure 5 displays each of these surface texture types at the same image scale while Figures 9-15 show multiple examples of each texture.

Knobby. This category of layer textures includes layers whose surface contains knobs or small hills (Figure 6). Knobby layers are identified in 26 images and occur throughout the NPLD. Individual knobs range from 20 m to 70 m in width. The spacing between knobs can range from 15 to 50 m. Multiple knobby layers can be seen on a single trough wall and at multiple elevations. These layers tend to
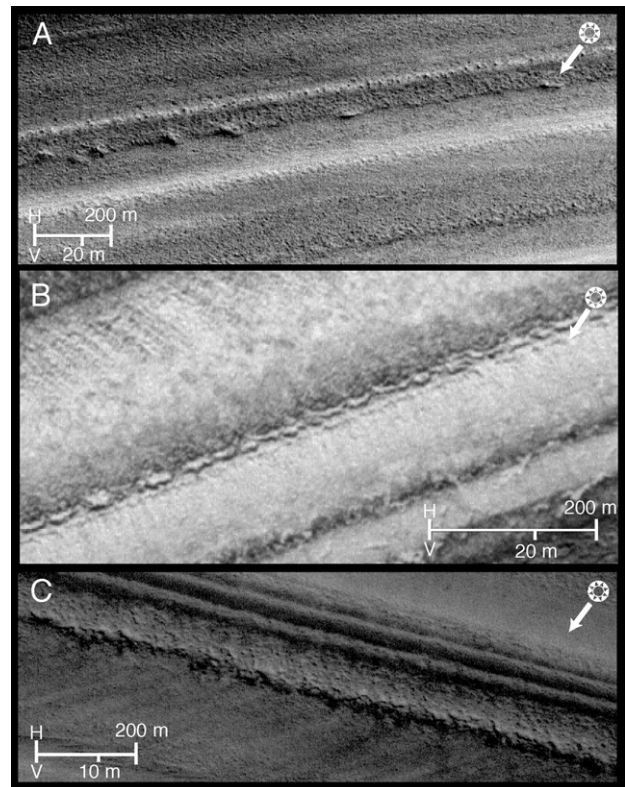

Figure 6. Knobby layers A) subframe of M00/00163 B) subframe of M00/01754 C) subframe of FHA/01515. Sun direction is indicated by arrows. Scale bar indicates the horizontal scale derived from the image on the top and vertical scale derived from the MOLA topography data on the bottom. (figure6.png)

be very bright relative to other layers within the same image.

A distinctive knobby layer referred to as a "marker bed" by Malin and Edgett (2001) and Kolb and Tanaka (2001) is found in several troughs around 80°E longitude and is characterized by knobs with average widths of 15 m and lengths of ~10 m (Figure 7). The marker bed is found in a number of locations throughout this region and extends over several hundred kilometers. It is usually located ~200 m below the top of the trough.

Pitted. Pitted layers are characterized by the presence of clear pits, ranging in size from 3 to 20 m in diameter, although a few over 40 m in diameter have been observed (Figure 8). The spacing between puts can range from 5 m to 15 m. Pitted layers are few in number, identified in only 17 images. Individual pits can be roughly circular or have an irregular shape. These layers are among the darkest observed in the images. The pitted layers have larger and more clearly-defined pits than the rough layers, discussed below.

Rough. Another texture observed in the NPLD is characterized by an uneven surface (Figure 9); these surfaces are not dominated by pits or knobs alone, but contain both features closely packed (Figure 5). This texture is the one most frequently observed in the NPLD (35 images). Rough texture is observed extending across multiple layers; the size of the pits and knobs frequently change at the transition
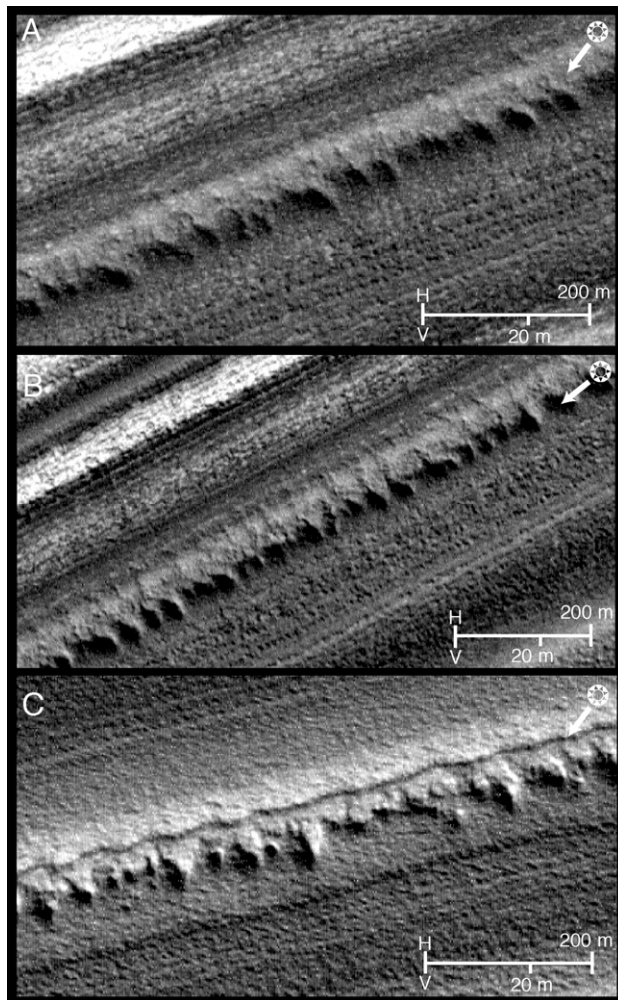
Figure 7. The marker bed. A) subframe of M00/01754 B) subframe of M00/02100 C) subframe of M00/02702. Sun direction is indicated by arrows. Scale bar indicates the horizontal scale derived from the image on the top and vertical scale derived from the MOLA topography data on the bottom. (figure7.png)

Figure 8. Pitted layers, arrows point to pits. A) subframe of M02/02431 B) subframe of M00/01754 C) subframe of R01/01449. Sun direction is indicated by arrows. Scale bar indicates the horizontal scale derived from the image on the top and vertical scale derived from the MOLA topography data on the bottom where concurrent MOLA data was available. (figure8.png)

between layers. These layers usually range in brightness from medium to dark.

Laminated. Laminated layers are a distinctive section of layers found in 22 images and characterized by alternating thin bright and dark layers (Figure 10). Each individual layer within the section ranges from 5 m down to the limit of resolution. A close inspection of the bright layers (Figure 10c) reveals that they are frequently made up of elongated knobs with widths ranging from the limit of resolution to continuous across the width of the image (up to ~4 km). Multiple sections of laminated layers can be found within a single image. Surficial frost deposits bring out the contrast between the two types of layers that make up the laminated layers (Figure 10c and d).

Imbricated. The final category of layer texture is only observed in 3 images. It is similar to the laminated texture; however, instead of parallel layers of bright and dark, the
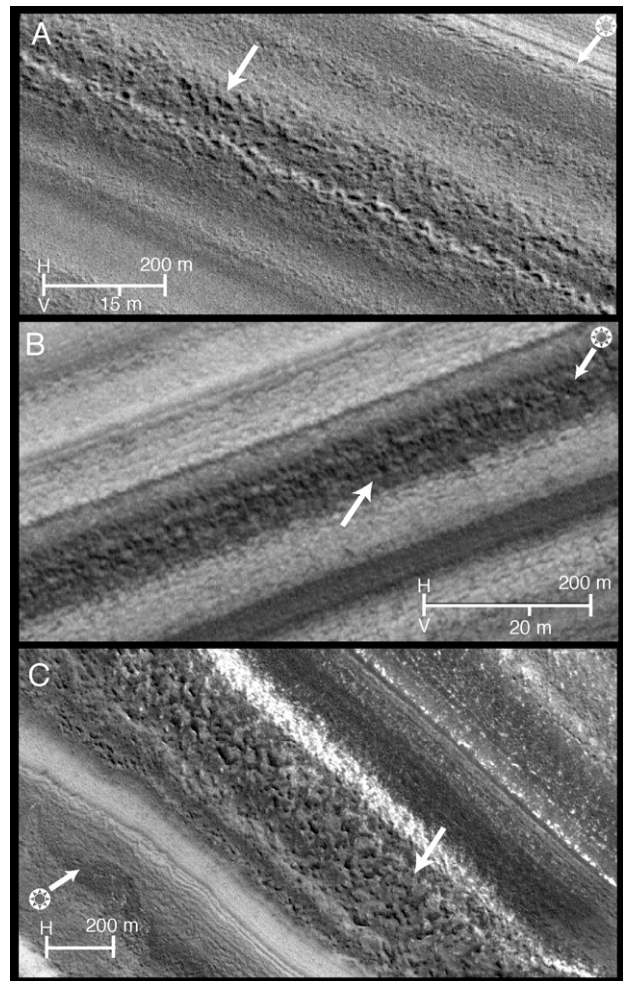
thin knobbed layers are non-parallel and superficially resemble cross-bedding (Figure 11). Again, surficial frost brings out the details of this layer type. This layer type is observed towards the base of the trough wall.

Deformational features

Previous examinations of high-resolution images located around the NPLD have found possible but not definite evidence of layer deformation in the form of irregular or wavy layers (Malin and Edgett 2001). Figure 12 shows one such image; it can be difficult in this image to tell if wavy layers are a product of deformation rather than erosion. We therefore look for layers with features characteristic of brittle deformation such as reverse faults. We searched for deformation in layers near the base of the NPLD where the maximum shear stress should be felt; based on terrestrial experience, we expect that any deformation present will be
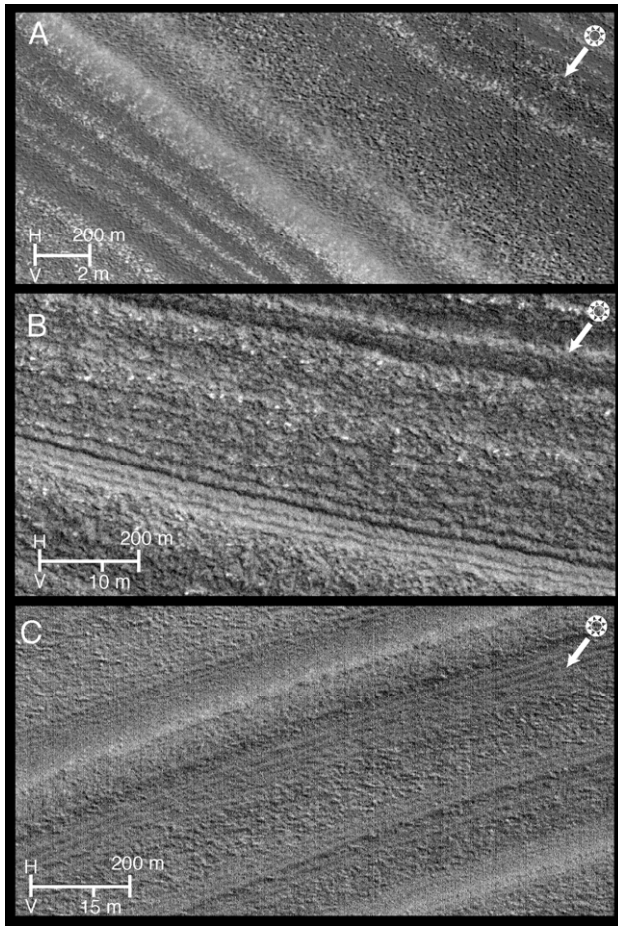
Figure 9. Rough layers A) subframe of M01/00034 B) subframe of FHA/01596 C) subframe of M02/02744. Sun direction is indicated by arrows. Scale bar indicates the horizontal scale derived from the image on the top and vertical scale derived from the MOLA topography data on the bottom. (figure9.png)

Figure 10. Laminated layers A) subframe of M02/00061 B) subframe of M00/01714 C) subframe of M00/00024 D) subframe of M00/01733. Sun direction is indicated by arrows. Scale bar indicates the horizontal scale derived from the image on the top and vertical scale derived from the MOLA topography data on the bottom where concurrent MOLA data was available. (figure10.png)

Figure 11. Imbricate layers A) subframe of M00/01754 B) subframe of M02/00747 (possible imbricate layer indicated by arrow). Sun direction is indicated by arrows. Scale bar indicates the horizontal scale derived from the image on the top and vertical scale derived from the MOLA topography data on the bottom. (figure11.png)

due to compression. The troughs that cut the deepest into the NPLD are located towards the deposit margins; a systematic survey was carried out searching through the high-resolution MOC narrow angle images located in these troughs.

Examination of one hundred and eighty three images around the NPLD (Figure 13; Table 2) reveals nine images containing layers with brittle deformation features and nineteen images with possible brittle deformation features. Three images located in the same trough near 83°N and 94°E contain a layer that appears to have been folded and locally faulted and overthrust (Figure 14 a-f). The layer, located towards the base of the trough at an elevation of about –3750 m, is ~1 m thick (the shallow slope of the trough makes it appear thicker in the images). The layer does not occur at the very bottom of the trough, and so is unlikely to be sand dunes. Individual segments of the layer range from ~90 m to ~260 m in length, averaging ~160 m. The edges of most segments are rotated away from the neighboring segments, oriented at an angle to the plane of the layer; this is consistent with motion along a fault due to shear stress. An additional image located at 83.3°N and 98.3°E (Figure 14 g, h) in a
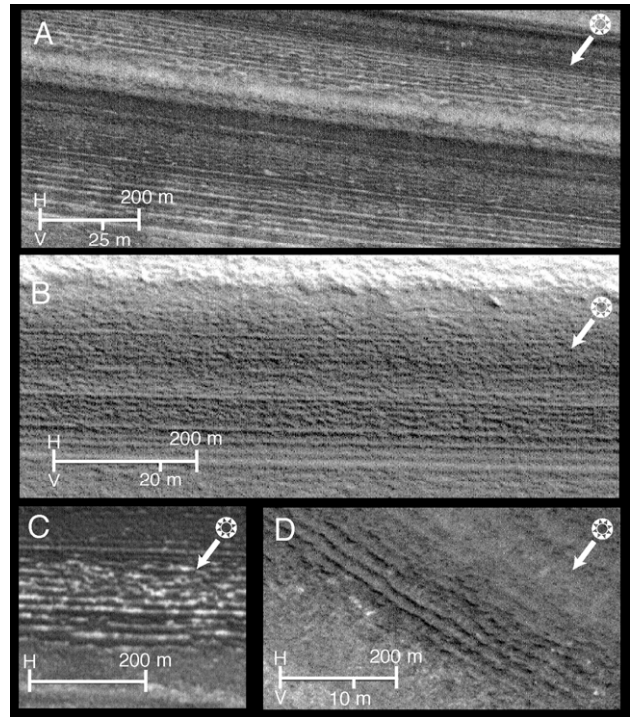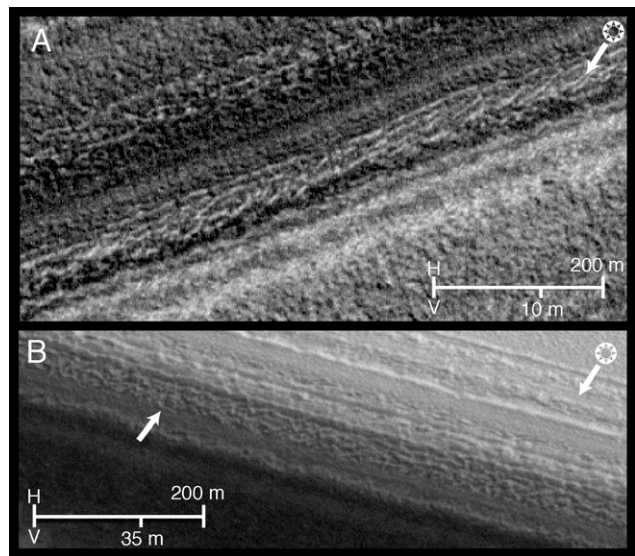
Figure 12. Possible layer deformation identified by Malin and Edgett (2001) in subframe of image M00/01925, near 81.4°N, 86.9°E. Sun direction is indicated by arrow. Scale bar indicates the horizontal scale derived from the image on the top and vertical scale derived from the MOLA topography data on the bottom. (figure12.png)
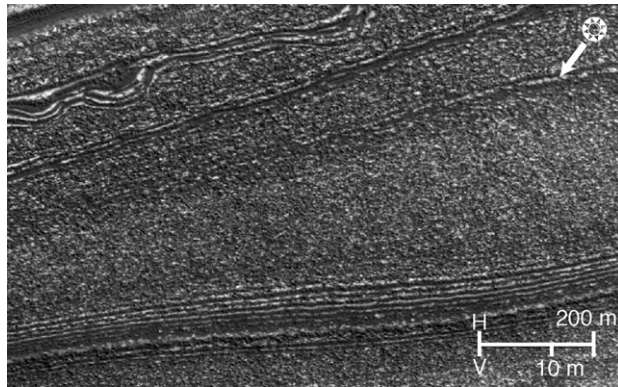
neighboring trough also has a layer with brittle deformation features. The segments in this layer average ~120 m length and are also rotated away from the layer plane. Additional, similar features are found in Figures 15 and 16. A layer in the middle of Figure 15 (indicated by arrow) appears to be faulted into segments and each segment rotated away from the layer plane. Each segment is approximately 100 m thick. Lower down, several layers are wavy in appearance, while another layer is broken into segments (indicated by arrows). Each segment is upwarped slightly at one end.

Clear evidence of faulting can be seen at the base of a trough in one image (Figure 17). A layer near the bottom of the trough contains three low angle reverse faults (indicated by arrows). Neighboring layers also appear fractured or deformed, allowing us to trace possible fault planes (indicated by dashed lines).

An unusual layer is observed in the bottom of a trough located at 84.8°N, 124.1°E (Figure 18); this layer may contain a fault. Unfortunately, only a small portion of this layer is exposed in the image. Nevertheless, there is evidence for thinning of the upper layer, topography on the basal contact, stratigraphic differences across the structure, and an apparent fault-like ramping.

Unconformities

Our search of several hundred NPLD images (Figure 4, 13) revealed 10 locations containing potential angular unconformities, all located between 4° and 40° E longitude (Figure 19). We consider each of these features to be a candidate angular unconformity due to the fact that each contains a sequence of layers that appear to be truncated by another sequence of layers oriented at a different angle. It is not clear how many of these features are due to an actual angular unconformity and how many are merely due to topographic effects making conformable layers appear non-continuous in the images. All images found containing these features were taken after the MOLA instrument stopped acquiring topography data; thus there is no concurrent
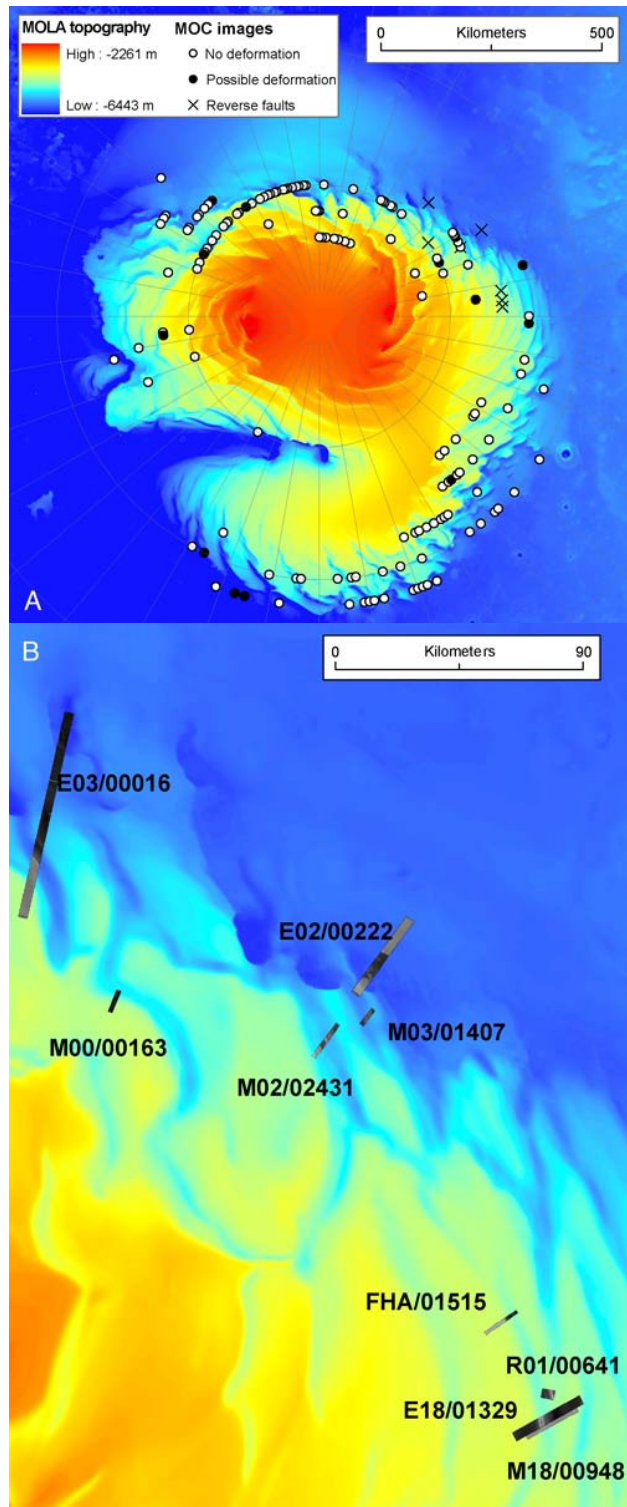

Figure 13. A) Locations of MOC images used in the deformation analysis superimposed on the north polar cap. B) Locations of images showing evidence of brittle deformation. (figure13a.png, figure13b.png)

topography measurements for these images. Overlaying the images on MOLA gridded data proved inaccurate due to the uncertainties in alignment and pointing between the two instruments. Nevertheless, it is difficult to create such layer
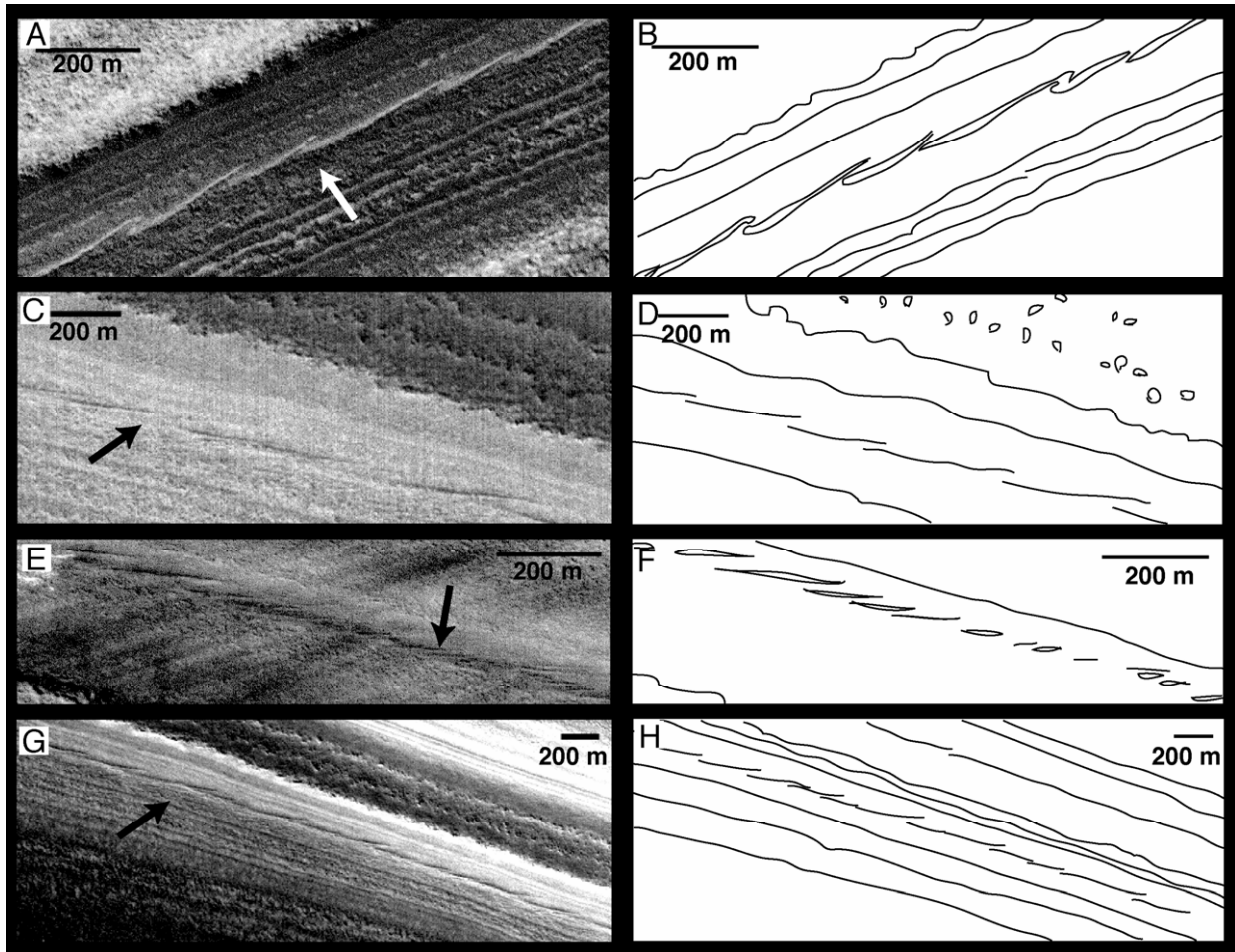
29

Figure 14. Examples of proposed thrust faulting in the PLD. Arrows point to the layers with the fault-like features. A) Subframe of R01/00641. B) Sketch of R01/00641. C) Subframe of M18/00948. D) Sketch of M18/00948. E) Subframe of FHA/01515. F) Sketch FHA/01515 G) Subframe of E18/01329. H) Sketch of E18/01329. (figure14.png)
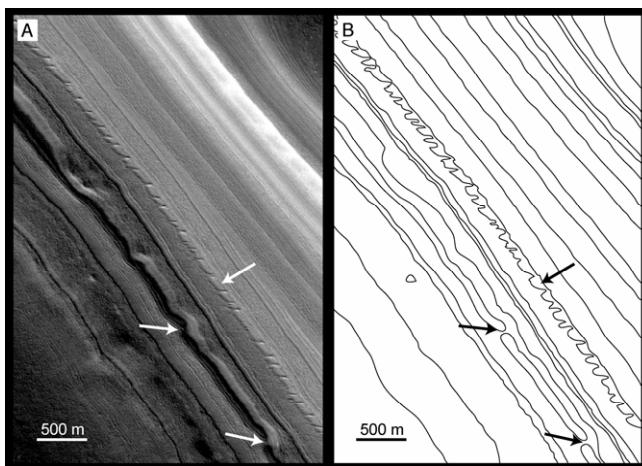
Figure 15. Example of proposed deformation in the PLD. A) Subframe of E03/00016. B) Sketch of E03/0016. Located at 84.1°N, 136.1°E. Arrows point to features of interest discussed in the text. (figure15.png)
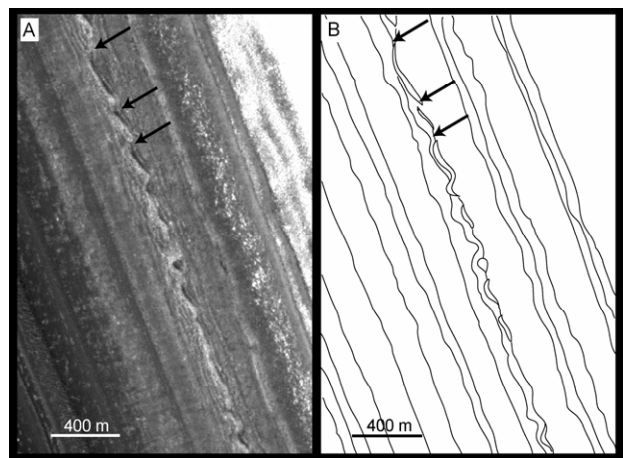

Figure 16. Example of proposed deformation in the PLD. A) Subframe of E01/01357. B) Sketch of E01/01357. Located at 85.3°N, 241.8°E. A layer in this image is folded, and several folds have detatched (arrows). Neighboring layers are also deformed. (figure16.png)
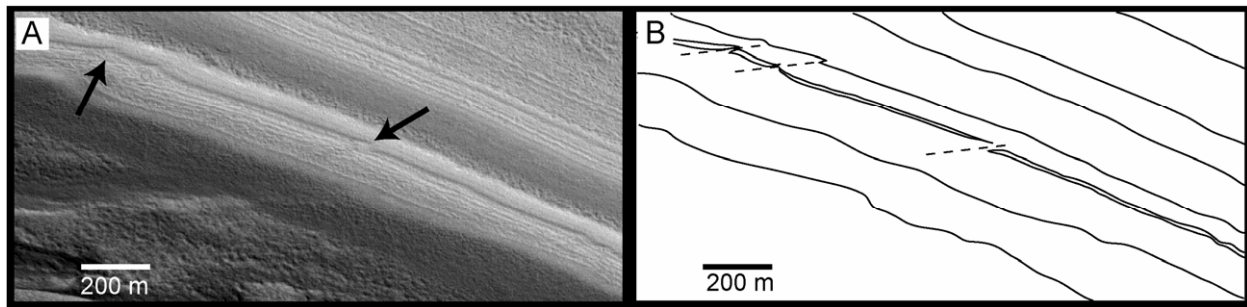
Figure 17. Faulting in the PLD. A) Subframe of M02/02431. B) Sketch of M02/02431. Located at 83.8°N, 115.8°E. A layer near the bottom of the trough contains three low angle reverse faults (arrows). Neighboring layers also appear fractured or deformed, allowing us to trace possible fault planes (dashed lines). (figure17.png)
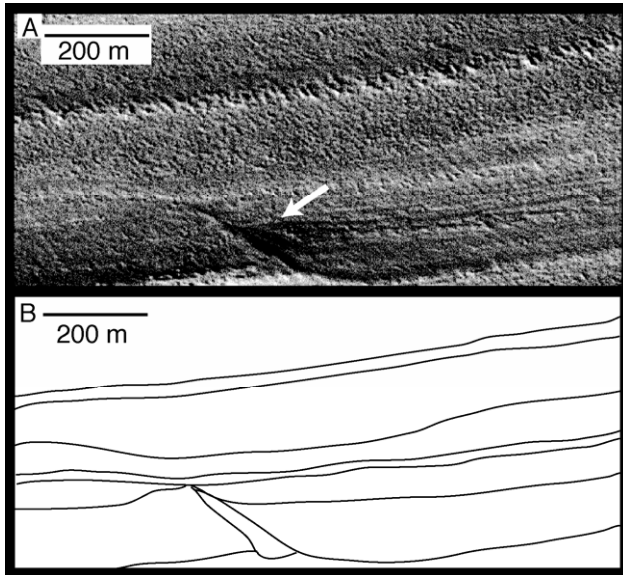

Figure 18. Example of proposed deformation in the PLD. A) Subframe of M00/00163. B) Sketch of M00/00163. The top of the trough is up. (figure18.png)

sequences such as those in Figure 19b, e, and l with topography alone.

Impact craters

The NPLD are remarkable for their youth – very few impact craters of any size have been identified, leading to age estimates of 0 – 100,000 years (Herkenhoff and Plaut 2000; Koutnik et al. 2002). The SPLD, in comparison, have a number of craters and an estimated surface age of ~10 Ma (Herkenhoff and Plaut 2000) to 30-100 Ma (Koutnik et al. 2002). This age discrepancy between the polar deposits is an important issue in Mars polar science and has implications for polar history and resurfacing processes. Any impact crater observed in the NPLD is unusual and should be examined with an eye to understanding how polar processes may affect their morphology.

An impact crater located within the NPLD at the base of a trough near 83.0°N, 94.5°E was identified in image M01/02447 by Koutnik et al. (2002). The crater is only partially visible in this image. It is completely visible in

R01/00641 taken during the extended mission of MGS (Figure 20).

Observations. Figure 20 shows the impact crater in R01/00641 and a sketch map of the crater and surrounding region. The crater is ~ 350 m in diameter. The rim is clearly visible but appears somewhat degraded. Interior to the crater are patches of bright material interpreted as frost. The surface immediately surrounding the crater is smoother than the neighboring terrain; this is interpreted as the remnants of an ejecta deposit. The ejecta deposit extends 50 to 200 m away from the crater rim in a lobate pattern.

An additional feature is observed within the NPLD in M02/04541, centered at 80.0°N, 331.4°E (Figure 21, indicated by arrow) and THEMIS visible image V12596003. This is a dark circular feature approximately 280 m wide. Layers of NPLD that enter this feature become curved in a geometry consistent with that of layers entering a depression. We interpret this circular depression as a potential impact crater; there is no evidence for a raised rim or ejecta material.

Discussion. In an analysis of lobate debris aprons on Mars, Mangold (2003) classified impact craters found on pitted ice-rich debris surfaces. The crater classifications include fresh, degraded, and ghost craters; the degraded craters are interpreted to have lost rim definition through sublimation and ice-flow processes. The impact crater in R01/00641 is similar in morphology to craters classified as relatively fresh (Figure 22). These are craters that may have experienced small amounts of degradation through sublimation and removal of material. The R01/00641 crater shows more evidence of ejecta materials than the craters on the debris aprons; thus, it may not have been exposed to sublimation for as long. This may be due to a younger age of the crater, changing climatic conditions at the poles, or to burial and subsequent exhumation of the northern crater by a volatile such as water ice or carbon dioxide. The potential crater in M02/04541, however, shows no evidence of a rim or ejecta deposit and so is similar in morphology to craters classified as degraded. The lack of distinct crater features may be due to a longer exposure to sublimation than the crater in R01/00641, either due to the age of the crater or to lack of burial and exhumation.   Additionally, the crater in M02/04541 is exposed on a trough wall instead of a trough bottom, and so may receive more insolation and thus
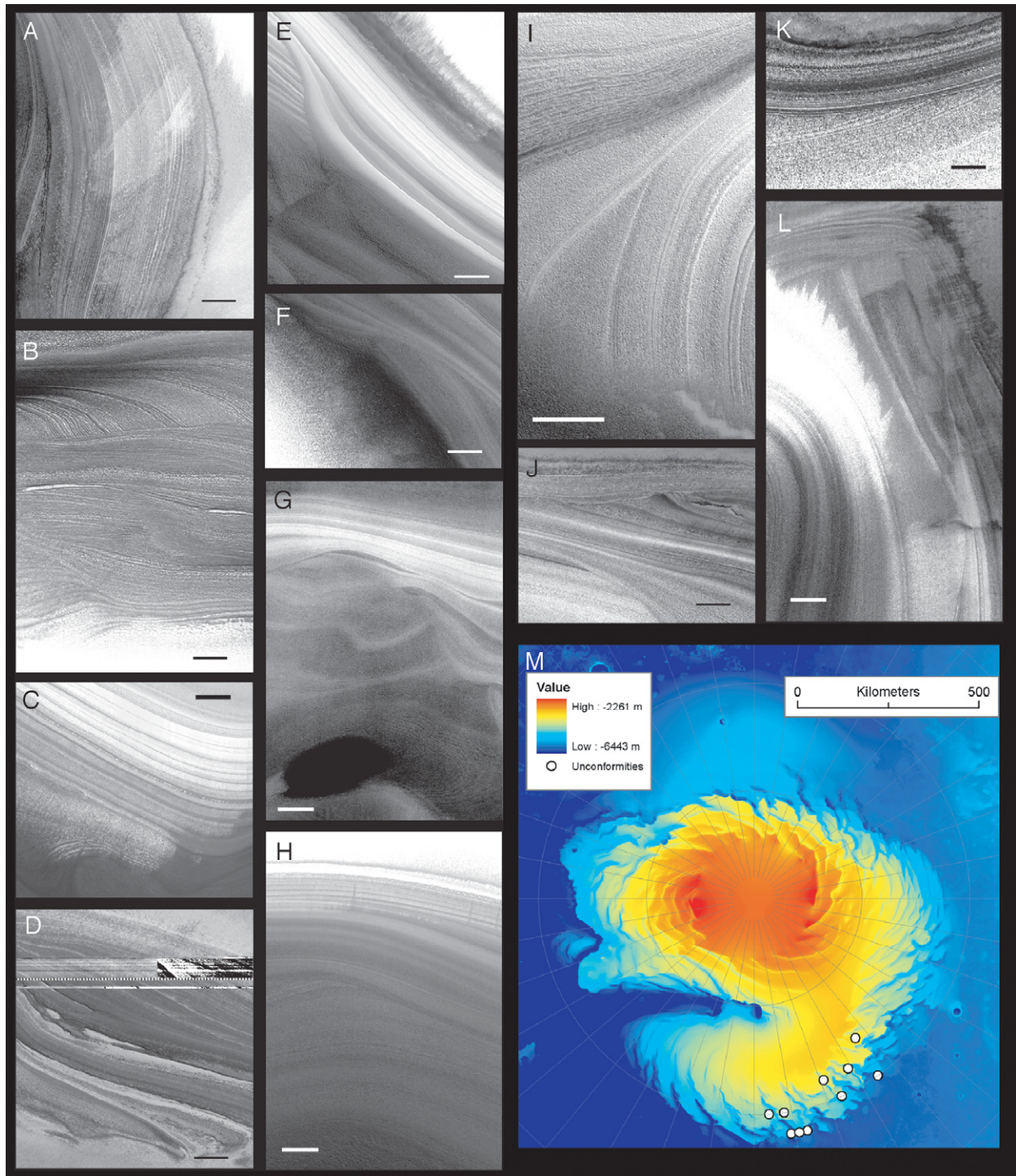
Figure 19. Proposed unconformities within the NPLD. All scale bars are 500 m. A) Subframe of E23/00801. B) Subframe of E23/01370. C) Subframe of R01/00556. D) Subframe of R01/00500. E) Subframe of R01/01188. F) Subframe of R01/01188. G) Subframe of E04/00826. H) Subframe of E22/01204. I) Subframe of E01/00703. J) Subframe of R01/00500. K) Subframe of R01/00437. L) Subframe of E04/00672. M) Location of images containing proposed unconformities mapped on gridded MOLA data. (figure19.png)

Figure 20. Impact crater within the northern cap. A) subframe of R01-00641. B) Sketch map. (figure20.png)

Figure 21. Proposed impact crater within the northern cap. A) Image M02/04541. Arrow indicates location of proposed crater. B) THEMIS visible image V12596003. (figure21.png)

undergo more intense sublimation than the crater in R01/00641.

NPLD Interpretations

Surface textures

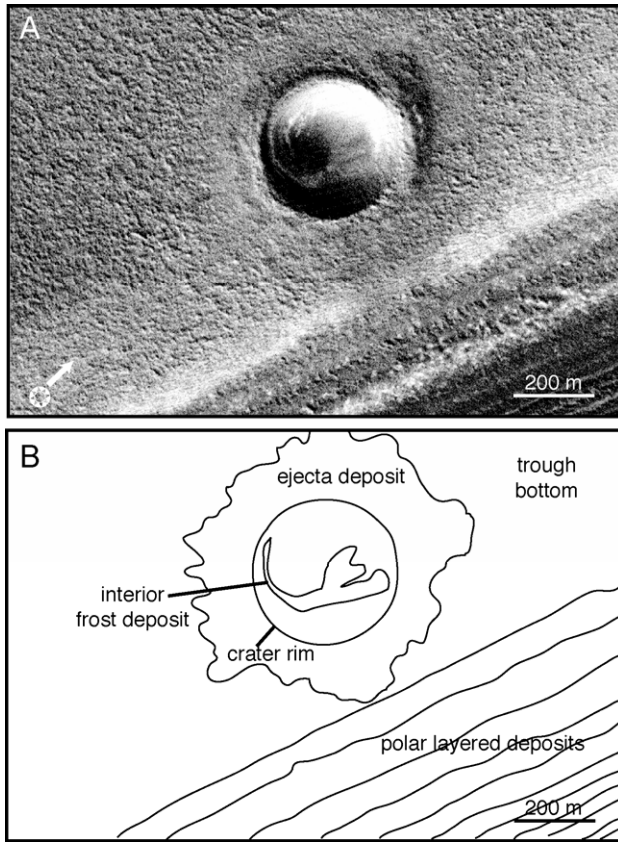The surface textures observed in the images may be due to physical properties of the layer itself or to post-depositional surface alteration. Here we explore how the various surface textures might be formed.

Strength of the layer. There are several ways in which a layer may be more resistant to erosion. It may be mechanically stronger and resist mechanical breaking up from abraiding particles carried by the local winds. Alternatively, it may be
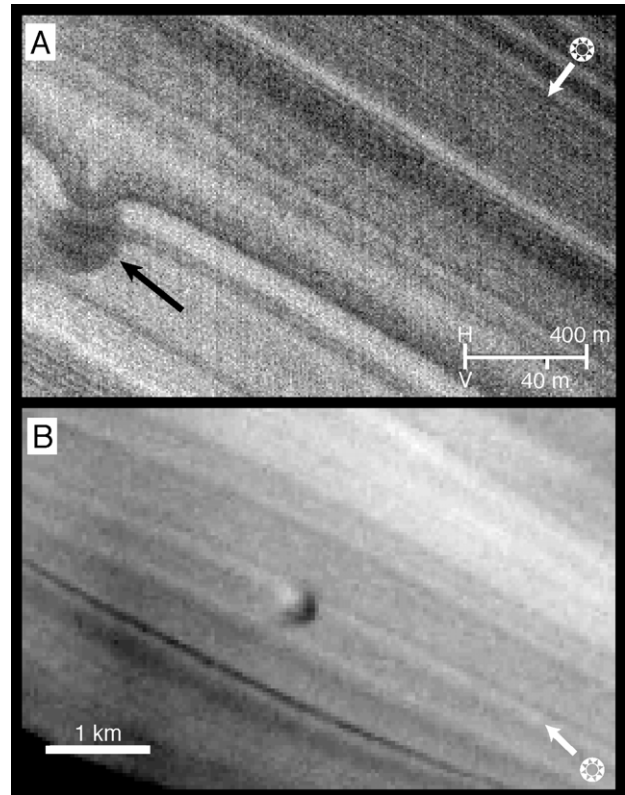
resistive to erosion through sublimation by forming a protective lag layer. In the latter case, dusty layers would be more likely to form a lag layer. However, Howard (2000) suggests that dust left behind on the trough wall by sublimation of NPLD is removed by the katabatic winds rapidly enough to prevent thick dust layers from forming as no erosional features and few wind erosional features have been observed on the trough walls. Thus, in the following discussion we concentrate on what may cause mechanically stronger layers.

Physical properties of the material making up the layer may control the surface exposure in the form of texture. A change in the material deposited in the marker bed could lead to a region of the layer having greater strength, and therefore
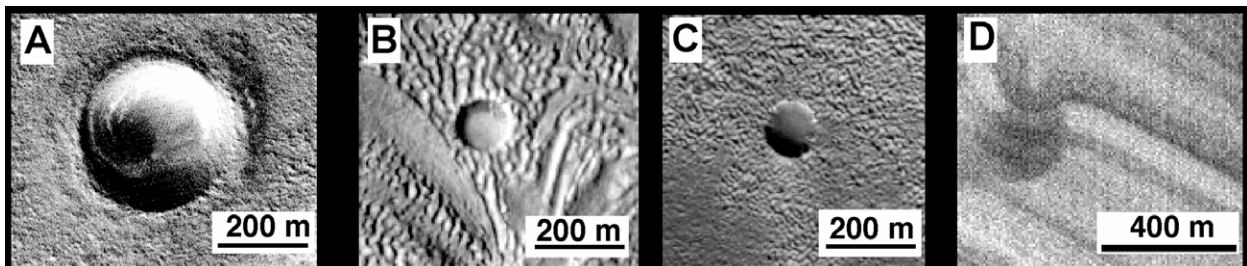

Figure 22. Craters into water-rich material. A) crater in the north cap. Subframe of R01/00641. B) Crater in lobate debris apron identified as "fresh" by Mangold (2003). Subframe of M00/02013. C) Crater in lobate debris apron identified as "relatively fresh" by Mangold (2003). Subframe of M10/02504. D) Possible impact crater in the north cap. Subframe of M02/04541. (figure22.png)

resistance to erosion, than the surrounding material. A layer with greater strength than the surrounding material tends to form ledges and benches on a slope surface; this could be the source of the knobby layers. A pitted layer may be due to relatively weak layer material. A series of layers made up of alternating strong and weak material could explain the laminated packets of layers. The alternating physical properties of the layers will lead to alternating resistant and erosive layers; the resulting slope variations may create the laminated appearance of these layers. If this layer packet experienced deformation and flow, the result might be the imbricated layer texture seen in several images. The changing strength of layers could be due to a change in the dust-to-ice ratio of the layer (e.g., Hofstadter and Murray 1990; Greve and Mahajan 2005) or in properties of the ice itself, such as grain size.

Grain size is an important physical parameter that has been much studied in terrestrial analysis of ice cores including ones from Greenland and Antarctica (Thorsteinsson et al. 1995). Changes in grain size can change the viscosity and strength of the ice (Thorsteinsson et al. 1997). Information on surface grain size can be used to characterize the interactions between the atmosphere and the polar surface (Nolin, 1998); and information on past grain sizes recorded within the ice can provide clues to the history of polar processes.

Grain size (Thorsteinsson et al. 1997; Goldsby and Kohlstedt 2001) and the type of bonds (Colbeck 1997) between grains control the strength of the ice layer and its response to stress and strain. If vertical compression is the dominant stress system in the ice, as found in the upper regions of an ice sheet (Paterson, 2001), fine-grained layers will be harder and flow less readily than coarse-grained layers (Thorsteinsson et al. 1997). If, however, the stress system is dominated by simple shear, as found in the lower regions of an ice sheet (Paterson, 2001), the fine-grained layers will shear and flow more rapidly (Thorsteinsson et al. 1997). Thus, in the upper regions of the NPLD, fine grained layers are expected to be strong whereas in the lower regions where simple shear dominates the stress system, fine grained layers are expected to be weak. As the magnitude of stress changes, the ice enters different creep regimes (in order of decreasing stress: dislocation creep, grain boundary sliding-limited basal slip creep or "superplastic flow," and basal-slip limited grain boundary sliding) in which the creep mechanisms are sensitive to grain size (Goldsby and Kohlstedt 2001).

Terrestrial ice deposits commonly are made up of layers that display different characteristics such as physical, thermal, and optical properties; each layer tends to be homogenous because it was deposited by relatively uniform snowfall. The homogeneity tends to be preserved through all subsequent metamorphism caused by weather conditions, ice particle arrangement, and gravitational loading from overburden (Zhou et al. 2003 and references therein). Recrystallization of ice grains occurs within polar ice sheets in response to changing temperatures and stress and strain conditions in the ice and is an ongoing process (Thorsteinsson et al. 1995 and references therein; Colbeck 1997).

Kieffer (1990) modeled rates of grain growth in the north residual cap and found several orders of magnitude difference in rates from the surface to depths of ~ 1 km (~1 to 1000 μm^2/yr). Observations of terrestrial ice cores at depths greater than 1 km indicate several factors that cause variations in growth rate (Thorsteinsson et al. 1995). Three regimes of recrystallization at different depths within a column of ice have been proposed (Figure 23). In the upper regime, surface tension effects cause pressure differences across grains, leading to the slow migration of grain boundaries and grain growth (Thorsteinsson et al. 1995). Larger crystals grow at the expense of small crystals, and the average crystal size increases linearly with the age of the ice (Thorsteinsson et al. 1997). In dry snow, rounded grains of ice grow slowly and build intergranular bonds, forming a neck where grains contact each other. This sintering process gives the ice strength. Sintering is a slow process, and cannot occur when a faster process of ice evolution if available. Large temperature gradients cause rapid growth of dry snow grains and thus when such gradients are present, sintering cannot occur (Colbeck 1997). In the middle regime, increasing strain within the ice causes the crystals to bend and eventually break apart. This acts to counter the slow migration of grain boundaries, limiting grain growth. In the lower regime, grain boundary migration occurs at high velocities due to the high age and high temperatures of the ice and the grain size grows again (Thorsteinsson et al. 1995; Thorsteinsson et al. 1997 and references therein). Figure 23 also gives the depths at which these transitions have been observed in the Greenland Ice Core Project (GRIP) ice core and the equivalent depths scaled for martian gravity, assuming the overburden is entirely water ice. This is an extremely simplistic assumption as temperature and impurity content differences between the two deposits will affect the depths of the recrystallization regimes as well.

Impurities in ice are thought to influence the speed of grain boundary migration; soluble impurities such as chloride or sodium ions slow boundary migration and grain growth (Alley et al. 1986; Thorsteinsson et al. 1995). Theoretical analysis indicates that a high content of insoluble impurities such as volcanic ash or dust are required in the ice to slow boundary migration; observations indicate that dust concentrations must be high enough to cause visible changes in snow albedo before grain sizes are affected (Alley et al. 1986). Given the range of brightnesses of layers within the martian polar deposits, it is likely that there are enough impurities such as atmospheric dust within individual layers to have indeed affected grain size.

Normal crystal growth rate is dependent on temperature and the initial grain size; initial grain size is dependent on the conditions under which the layer originally formed (e.g., Thorsteinsson et al. 1997; Nolin 1998; Nolin and Dozier 2000). Therefore, the grain size within a layer of ice indicates the climatic conditions under which the layer formed in addition to the thermodynamic processes at work within the NPLD.
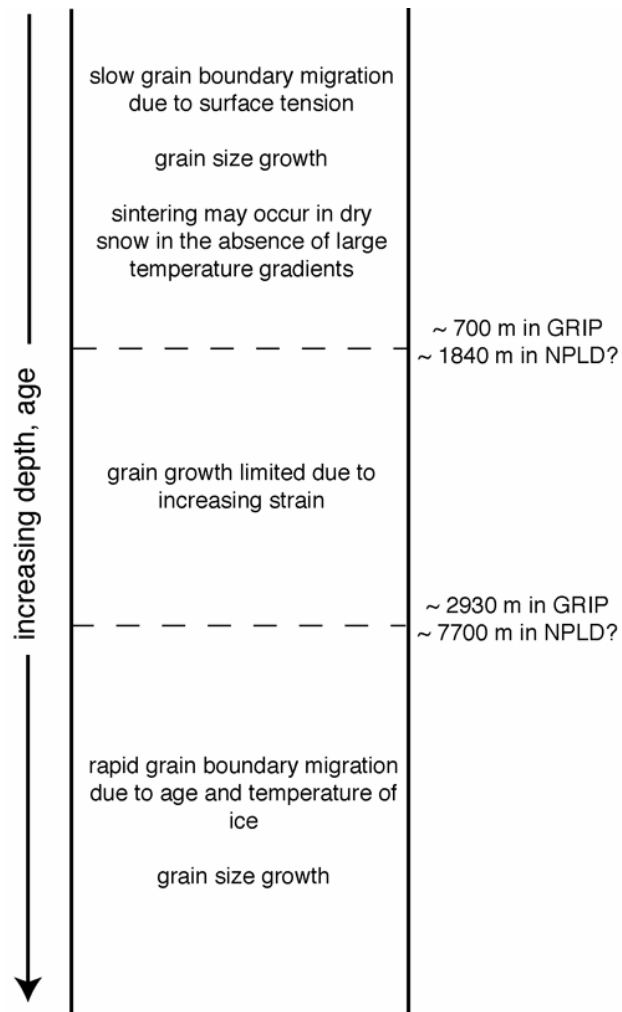
Figure 23. Proposed three regimes of ice grain size within an ice sheet, based on the research of Thorsteinsson et al. (1995, 1997). Numbers indicate depths where transitions between regimes are observed in the terrestrial GRIP ice core and the equivalent depths for the NPLD when simply scaling for martian gravity.

Based on our understanding of the behavior of grain size in terrestrial polar ice sheets, we expect that the martian deposits should contain a variety of grain sizes. These grain sizes have been influenced by the same changing climate conditions and ice/dust ratios that are recorded by the polar layered deposits. Grain size in the martian deposits should generally increase with depth as the ice increases in age; deviations from this trend should correlate with climate change but be modulated by other factors such as composition, impurities, and the range and absolute values of temperature.

On Earth, a wide range of ice grain sizes is observed in a single ice core; the terrestrial ice record reveals that grain size is correlated to climatic (and thus orbital) conditions at the time of snowfall. In Greenland ice cores, larger crystals are associated with warm spells in climate. A sudden transition to small grain sizes corresponds to a catastrophic cold event in the climate record (Thorsteinsson et al. 1995). Therefore, the relative strengths of ice layers on Mars could

vary with depth as a function of climate-induced grain size variation, and this prospect should be kept in mind when considering the physical properties of the martian polar deposits.

Evidence for the formation of pitted layers through erosion of weaker material such as a coarse grained layer in a compression-dominated zone of the NPLD or a dusty layer is found in image R01/01449 (Figure 24). In this image, the changing topography across the image results in NPLD being exposed on 2 slopes (similar to the image in Figure 7), a shallow slope located in the upper portion of Figure 24a and a steeper slope in the middle portion of Figure 24a. The dark material in the lower region of Figure 24a is the BU. Individual layers of NPLD can be traced across both slopes. The pitted terrain in Figure 11c is found in the left side of the shallow NPLD exposure (indicated by arrow in Figure 24b) and is part of a dark layer exposed on the steeper slope (identified by arrow and dashed line in Figure 24b). A sketch map of this image (Figure 24b) highlights the relationship. The dark sections of this layer may be regions where the layer has eroded away, leaving a shadowed overhang. Additional features indicated by small arrows in Figure 24a may be due to wind erosion.

The marker bed (Figure 7) is an extremely unusual layer since it forms a distinctive sawtooth ridge or overhang; it must be made up of a mechanically strong material compared to the other layers within the NPLD. It is comparatively thick in the troughs near 80°E and yet is not obvious elsewhere. Therefore it may be deposited unevenly through the NPLD. Only one marker bed has been observed thus far in the polar layers; it may record an unusual event in martian climate history. Such an event might include outgassing of H_2O through an impact or a volcanic eruption, or a sudden climate shift causing the migration of volatiles
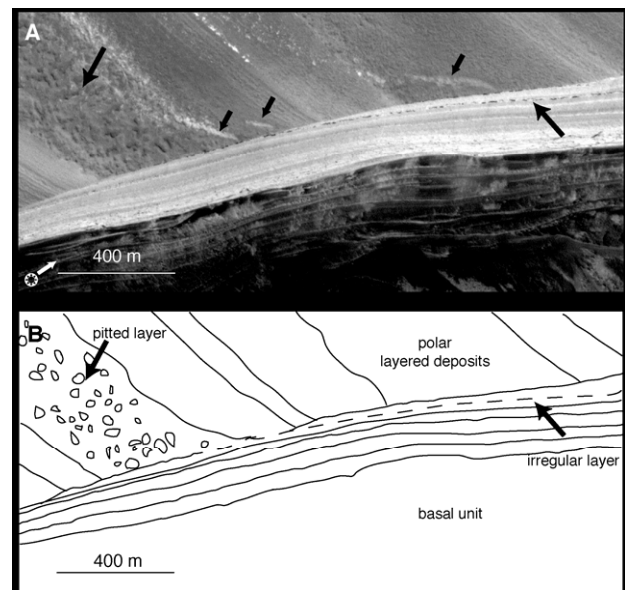

Figure 24. Pitted layer within R01/01449. A) subframe of R01/01449. B) Sketch map. Sun direction indicated by arrow. (figure24.png)

from the mid-latitude or equatorial regions to the pole.

Milkovich and Head (2005) and Milkovich et al. (2006) have examined the polar layered deposits for climate signals using Fourier analysis; they identified a "no periodic signal" zone ~300 meters below the deposit surface where such signals are absent and interpreted it as the lag deposit from the most recent migration of volatiles to the mid-latitudes due to a decrease in obliquity approximately 0.5 million years ago. The marker bed is located immediately above this zone, implying that it formed in the last 0.5 million years. As discussed in Section 3.3, near polar volcanic structures on Mars may be as young as 1-20 million years old (Garvin et al. 2000). Recent as this volcanism may be, it is still too old to be a source for a strong, ice-rich marker bed. Impact cratering is a plausible alternative, as models show that material ejected into the atmosphere with speeds in excess of 3 km/s by a significant impact above 45° latitude will ultimately end up at the opposite polar region. For example, model calculations show that Lyot, a 220 km diameter crater, could have deposited meters of impact glass and melt at the southern polar regions (Wrobel and Schultz 2004).

An alternative hypothesis is that the climate shift 0.5 million years ago was a gradual transition rather than a sharp event. In this scenario, volatiles began to migrate to the polar regions as obliquity decreased. Layered deposits continued to form above the lag deposit, but once obliquity reached levels lower than a critical value, a large amount of volatiles moved to the polar region and formed the marker bed. The amount of water available to form the NPLD dropped, and the layers deposited since then have had a much higher dust/ice ratio.

Modeling of transport of water under varying orbital parameters indicates that to a first order the net water removed from the polar deposits depends on summer polar insolation which depends in turn on obliquity, eccentricity, and argument of perihelion. For circular orbits water is removed from the deposits at 35° obliquity while for an orbit with current eccentricity and argument of perihelion water is removed at 30° obliquity; other orbital configurations require obliquities up to 40° (Levrard et al. 2004). Thus, it may be possible that changes in orbital parameters beyond obliquity control deposition of ice at the polar regions as well, and so the above scenario could be caused by several orbital parameters gradually coming into an alignment favorable to rapid ice accumulation at the pole.

If this scenario is true, then we would expect to see a similar marker bed at very deep levels in the cap representing a similar climate transition from ~2.5 million years ago at the time of the previous shift in maximum obliquity (e.g. Head et al. 2003). Such beds have not yet been identified, which may indicate that this hypothesis is incorrect or that the layers exposed in the images are all younger than 2.5 million years and the marker bed from this climate shift is buried within the NPLD.

Unusual composition of layers. Water ice is a major component of the NPLD (e.g., Mellon 1996; Kargel and Lunine 1998), but the presence of CO_2-rich layers in the form of CO_2 clathrate hydrate layers or layers of solid CO_2 is theoretically possible since these materials should be stable at temperatures and pressures found within the NPLD (e.g., Jakosky et al. 1995; Mellon 1996). Several researchers find that clathrate is thermodynamically more likely to be found in the polar deposits than CO_2 ice (Miller and Smythe 1970; Kargel and Lunine 1998). However, calculations taking into account the likely presence of dust, salts, and layers limit the amount of CO_2 in the form of clathrate to a few 10s of mbar (Mellon 1996).

Both clathrate and solid CO_2 are unstable at the surface of the north polar deposits under current atmospheric conditions (Miller and Smythe 1970; Kargel and Lunine 1998). However, clathrate layers could form under several conditions. Clathrate may form in the atmosphere and precipitate out in small amounts; since solid CO_2 is stable at high altitudes clathrate must be stable at lower altitudes (Miller and Smythe 1970). Clathrate may also form on the surface of the NPLD by the reaction of water ice with CO_2 vapor; this process has been proposed for the current southern polar deposits (Kargel and Lunine 1998). Clathrate is stable at depths of 1.5 m in the NPLD under present conditions (Kargel and Lunine 1998). If clathrate were exposed in the trough walls it would decompose into gaseous CO_2 and water ice. The CO_2 would vent explosively out of the trough wall and drive the water ice fragments out as well (Ross and Kargel 1998). This process is endothermic at polar surface temperatures (Miller and Smythe 1970) so we do not expect any violent run-away phenomena and associated morphological features. Sublimation and decomposition would gradually propagate into the exposed layer until the layer is sealed with water ice. Decomposition of clathrate produces H_2O ice that can seal the decomposing layer effectively. Thus, we would anticipate bands of local depressions in the trough surface in association with the layers of material unstable at current atmospheric conditions. The rough textures may be cavities formed in this manner.

For the clathrate layer to be preserved within the cap in order to be the source of the variations in surface texture, 1.5 m of water ice must be deposited before the clathrate can decompose, requiring rapid deposition in a single season. This could occur as a result of the release of volatiles through volcanic activity or groundwater breakout (Berman and Hartman 2001). Such a large and rapid deposit of water ice would require a sudden, large influx of water into the atmosphere for transport to the poles. The probable rarity of water-releasing events combined with the small amounts of CO_2 likely to be contained within the deposits implies that such clathrate layers should be extremely rare.

Erosional surface. The surface texture of the layers may be due to removal of material from the surface exposure, which in turn is the result of physical characteristics of the layer itself. The rough texture observed throughout the NPLD is consistent with ablation hollows. This texture contains closely spaced, regular depressions and is found on at a number of locations and elevations. Rough textured layers vary in brightness, but are consistently among the medium to

darker layers in any image. Given the prevalence of rough textured layers throughout the NPLD, a suncup-like source for the rough texture is a more plausible alternative than the clathrate outgassing model.

The surfaces of terrestrial ice sheets and glaciers frequently have structures known as ablation hollows, suncups, or (in a more extreme form) penitentes (e.g., Rhodes et al. 1987; Betterton 2001; Herzfeld et al. 2003). These structures form small-scale relief on ablating ice surfaces. They typically take the form of a honeycomb-like network of evenly spaced and sized simple hollows bounded by ridges (Figure 25). These hollows often have a ridge-to-hollow relief of 0.3-6.0 m (Rhodes et al. 1987), although spikes up to 85 m have been observed (Betterton 2001). The spacing between hollows tends to be 0.4-0.6 m (Herzfeld et al. 2003). Ablation hollows are found at a range of elevations and occur on surfaces independent of inclination. The mottled terrain on Comet 19P/Borrelly has been proposed to contain ablation hollows (Britt et al. 2004).

Ablation hollows are thought to form through radiant heating of the surface due to direct or indirect sunlight (Rhodes et al. 1987; Betterton 2001) or through turbulent heat transfer in the atmosphere (Rhodes et al. 1987). The second method requires warm atmospheric temperatures and so is unlikely to be applicable on Mars due to the limited convective cooling between the surface and the atmosphere (Hecht 2002). Under the radiant heating formation mechanism, sunlight causes the growth of these features due to the fact that the base of the depressions receive more reflected light than the ridges that surround it, causing the depressions to deepen. The presence of dust or dirt complicates the processes involved. As ice sublimates, any dust present will move in a trajectory perpendicular to the surface (e.g.
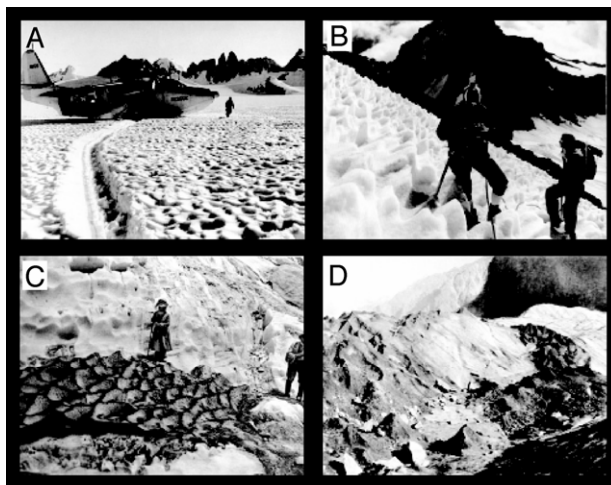

Figure 25. Ablation features on terrestrial ice sheets. A) Suncups on Taku Glacier, Coast Mountains, Southeast Alaska. From Post and LaChapelle (1971). B) Deep suncups in Disappointment Cleaver, Mount Rainer. From Post and LaChapelle (1971). C) Ablation hollows with dirt collected on the ridges; reportedly 12 to 18 inches high. From Workman and Workman (1909). D) Dirt cones approximately 20 to 40 inches high. From Workman and Workman (1909).
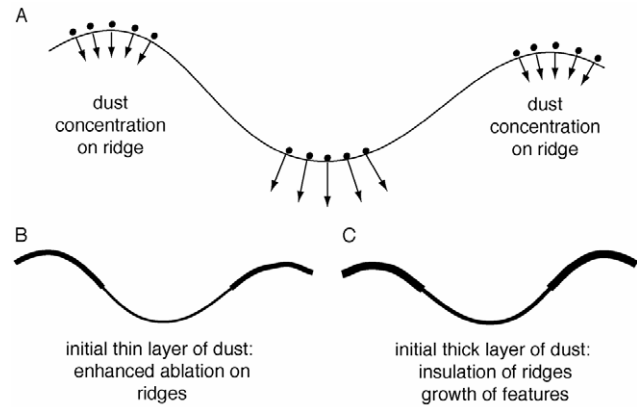

Figure 26. Formation of ablation hollows. A) Retreat of dust tangential to ablating surface causes concentration of dust particles on ridges. B) A thin layer of dust covering the surface will enhance sublimation on the ridges, causing the ablation hollows to be removed. C) A thick layer of dust covering the surface will insulate the underlying ice, causing the ablation hollows to be preserved.

Rhodes et al. 1987); thus the dust will concentrate on the ridges of the ablation hollows (Figure 26). Observations and modeling of the behavior of ablation hollows on dusty ice surfaces suggest that there is a threshold value of initial surface dust thickness that controls the evolution of the hollow; the value of this layer thickness is unknown (Betterton 2001). If the layer of dust on the surface is thinner than this value, then the dust acts to increase the amount of ablation on the ridges. Since the dust is concentrated on the ridges (Figure 26), more light is absorbed at the ridges and thus the ridges ablate faster than the hollows. This has the effect of erasing the ridges and removing the ablation hollows. However, if the layer of dust on the surface is thicker than the threshold value, the dust acts to insulate the underlying ice. In this case, since the dust in concentrated on the ridges, they are more protected than the hollows. Thus, the hollows ablate faster than the ridges. This has the effect of causing the ablation hollows to grow and be preserved (Rhodes et al. 1987; Betterton 2001). There are therefore three modes of ablation hollow formation: on pure, clean ice, which allows growth and preservation of the features, on lightly dusty ice, which allows temporary formation of ablation hollows but not their preservation, and on very dusty ice, which allows growth and preservation of the features.

Since ablation hollows form on a range of ice surfaces, including both dirty and clean ice, it is likely that they would also form on surfaces in the NPLD. Since individual layers within the NPLD contain a range of dust contents, it is possible that some layers will contain enough dust to allow the growth and preservation of ablation hollows while others will not. Thus, in any sequence of NPLD it is likely that some layers will be covered in ablation hollows and some will not. Based on our understanding of terrestrial ablation hollows, we predict that dark layers are more likely to preserve such features since they probably contain more dust and thus are more likely to have enough dust to allow ablation hollows to be preserved. As described above,
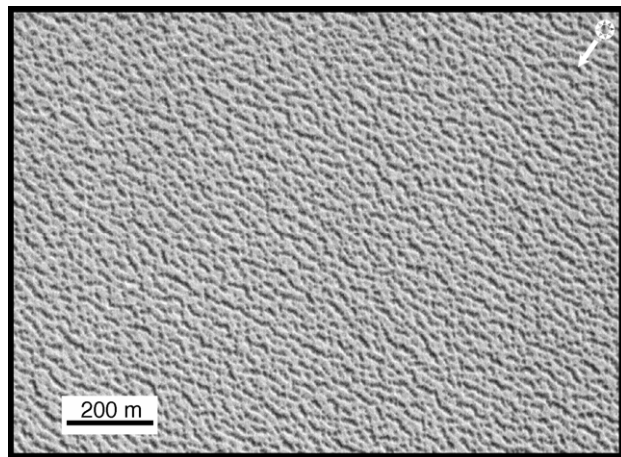
37

Figure 27. "Cottage cheese" terrain on the residual cap surface. MOC image CAL/00433.

Figure 28. Model of texture formation as a function of insolation-controlled dust accumulation.

ablation hollows on dust-poor layers are likely to form and then be removed, and therefore are less likely to be observed in the MOC images. While terrestrial ablation hollows are too small to be detected in the resolution of images available from Mars, it is possible that similar features on a larger scale may be observed in the NPLD.

The surface of the layer may be eroded before the layer is buried by later NPLD. Areas of the current residual cap have a small-scale hummocky appearance called the "cottage cheese" terrain (Figure 27) (Thomas et al. 2000); this terrain is characterized by pits 1-2 m deep and tens of meters across joined in roughly linear strings or depressions with preferential direction (Fisher et al. 2002). The lineations may be due to the evolution of surface pits by ice flow and/or katabatic wind erosion combined with differential ablation of volatiles on warmer south-facing slopes and deposition on colder north-facing slopes (Fisher et al. 2002). Once this surface is buried under the next accumulated layer of NPLD, the cottage cheese terrain may influence how this particular layer is exposed on a trough wall. For example, buried cottage cheese terrain may contribute to small-scale variations in layer thickness along a trough and may control how a layer erodes out of the trough wall.

Model for dust-controlled surface texture formation.

Several recent analyses of NPLD stratigraphy have focused on correlations with orbital frequencies (Laskar et al. 2002; Milkovich and Head 2005, Milkovich et al. 2006). Layer packets of 30 m thickness are observed in the upper approximately 300 meters of the NPLD; each packet is made up of multiple layers generally tending from light to dark (Milkovich and Head 2005) and likely corresponds to the "layer pairs" observed in lower-resolution Viking images (e.g., Thomas et al. 1992). These layer packets are likely due to precession-dominated insolation cycles influencing layer accumulation (Milkovich and Head 2005). Each layer texture approximately correlates with layer brightness; thus layer texture may be controlled by the physical effect of insolation on layer accumulation. If we assume that bright, knobby
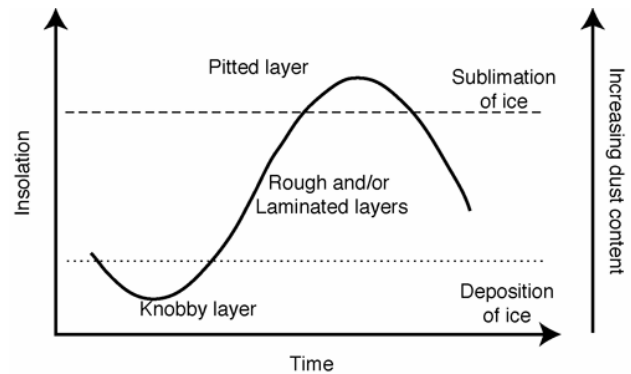
layers are dust-poor and the darker the surface, the more dust contained within the layer, we can form a simple model relating surface texture to insolation cycles (Figure 28).

Total insolation is controlled by the quasi-periodic orbital elements, including the combined effects of eccentricity, obliquity, and argument of perihelion (e.g., Laskar et al. 2002). We assume that at periods of low insolation, the most ice-rich layers will be deposited since the polar regions will serve to cold-trap water. As the insolation increases, so does the dust content of the accumulating layers. At some threshold value (dotted line in Figure 28), there is enough dust contained within the accumulating layer to preserve any ablation hollows that later form on the surface exposed on the trough wall. Thus, during periods of intermediate insolation, layers are deposited that will tend to develop rough surfaces under current conditions. Fluctuations in dust content due to the behavior of dust storms could lead to the development of laminated layers in this period as well. Finally, in some cycles insolation may increase enough to cause sublimation of the ice deposits (upper dashed line in Figure 28); this would concentrate dust in this layer that would erode differently and may produce the pitted layers. Because the amplitude of the insolation cycle varies over time (e.g., Laskar et al. 2002) these cycles are not exactly repeatable; therefore, a knobby or pitted layer may not form in each cycle. An important issue this model does not address is how the seasonal CO_2 cap interacts with layer deposition.

Deformational features

Initial examination of the geometry of the fault-like features discussed above indicate that they are oriented so the hanging wall is moving towards the margin of the NPLD; this is consistent with compression experienced at the margin of a flowing sheet of ice.

It is well-documented that terrestrial ice sheets of sufficient thickness can flow (e.g., Hambrey and Milnes 1975). Whether or not the NPLD has undergone flow in its history has been a matter of extensive debate, as no clear deformational feature have been observed, leading many researchers to conclude that the NPLD have not flowed (e.g., Hofstader and Murray 1990; Kolb and Tanaka 2001), while

models based on terrestrial glacial experience indicate that if the martian northern polar deposits are thick enough and the geothermal gradient at the base is high enough, they should flow as well (e.g., Clifford 1987; Fisher 1993, Fisher 2000; Nye 2000; Fisher et al. 2002; Greve et al. 2003; Hvidberg 2003; Greve and Mahajan 2005). However, the behavior of the polar materials is not known due to the unknown proportion of dust in the NPLD; the presence of dust can increase of decrease the viscosity of the ice, depending on the amount of dust and the mechanism of flow (e.g., Hofstader and Murray 1990). The effect of varying dust content on ice rheology is not well understood, especially for the low strain rates anticipated within the NPLD (e.g., Greve and Mahajan 2005) and is currently being explored in the laboratory (e.g., Goldsby and Kohlstedt 2001; Mangold et al. 2002). The presence of layers deformed by flow could provide insight into the strength and behavior of the NPLD as well as the conditions and style of deformation.

In a simple symmetric terrestrial ice sheet in temporal steady state, accumulation of ice in the center of the sheet and ablation of ice at the edges are constant. Mass balance requires that ice flows from the accumulation zone to the ablation zone. Ice and other material deposited in the accumulation zone move downward and are thinned by compression and shear flow (Figure 29a). Thus, layers internal to the ice sheet (for instance, dust or tephra) also get thinner and experience more shear as they get closer to the ice bed. In addition, if the ice at the very base if the sheet is at the melting temp, it must flow over the ground surface that underlies the ice sheet; the topographic relief of this surface may distort the layers (Fisher 1993).

What kind of evidence should we be looking for to determine where, when, and how much the ice flows? Ice flows by creep, or movement within or between individual ice crystals. The rate of ice creep is a function of shear stress and is affected by impurities such as the presence of dust within the ice (e.g., Hofstadter and Murray 1990; Durham et al. 1992). Most creep occurs in the lower region of an ice cap or glacier where the shear stress is greatest. When the ice cannot creep fast enough to allow the ice sheet to adjust its shape under stress, the ice can undergo brittle failure or fracture (e.g., Ramsay 1967; Patterson 1994). Basal sliding may occur if pressure melting permits a thin layer of water to form at the bed of wet-based glaciers. The combination of creep and basal sliding permits accelerated ice flow. In extremely cold environments, ice temperatures may lie below the pressure-melting point. Such cold-based glaciers move slowly and only by creep (Patterson 1994). Cold-based glaciers are common in Antarctica today and geologic evidence for former cold-based glaciers on Mars has been previously documented (Head and Marchant 2003; Shean et al. 2005). Calculations of basal temperatures for varying deposit compositions indicate that a wet-based polar deposit (undergoing basal melting) would require a geothermal flux in the upper range of current estimates and/or a significant portion of the NPLD to be made up of CO_2 in the form of clathrate (Kreslavsky and Head 2002). Whether an individual layer deforms in a brittle or ductile manner

depends on the dust content of the layer and the position of the layer with depth as the stress increases with depth in the NPLD.

Extensional zones within the ice can cause individual layers to thin (in the case of a ductile layer) or fracture (in the case of a brittle layer). A brittle layer surrounded by ductile layers will break apart, and the surrounding ductile material will flow around and into the gaps to form boudinage structures (Bennett and Glasser 1996).

Compression zones within the ice can cause fold-and-thrust features similar to those found at compressive plate boundaries on the Earth (Ramsay 1967). Folded ductile ice can also be detached from the underlying substrate along a bedding plane known as a décollement. Overthrusting reverse faults can further deform the folded ice (Bennett and Glasser 1996).

The state of stress (compressional vs. extensional) at the base of an ice sheet depends on whether the ice is accelerating or decelerating. This in turn depends on the thickness of the ice, the basal temperature of the ice, and whether the ice is located beneath an accumulation zone or an ablation zone. For a simple domical ice sheet, the interior regions experience extension while the marginal regions undergo compression (Figure 29b) (Bennett and Glasser 1996).

A major difference between the simple ice sheet described above and the NPLD is the presence of spiraling troughs cutting into the NPLD, exposing the layers of ice and dust. The walls of these troughs are much darker than the ice-
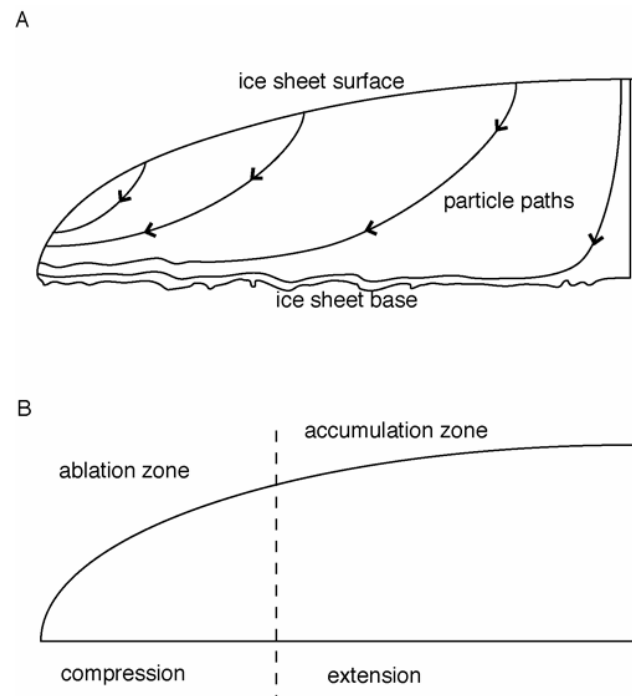
Figure 29. Properties of a flowing ice sheet. A) Internal layers within a flowing ice sheet. Note the deformation at the base of the sheet due to the underlying surface. B) Stress zones within a flowing ice sheet.

covered polar flats between troughs, which has led to the theory that ablation in the form of sublimation occurs on the equator-facing slopes while deposition occurs on the bright flat areas (Squyres 1979; Howard et al. 1982; Blasius et al. 1982; Fisher 1993, Fisher 2000). This process may cause the troughs to migrate poleward in a conveyor-like fashion (Squyres 1979; Fisher 1993, Fisher 2000; Fisher et al. 2002). Thus, the troughs may be moving inward on top of the ice which is moving outward (Fisher 1993). Modelling work by Hvidberg (2003) leads to another model of flow in the NPLD; her finite element ice flow model to calculate flow rates and trajectories assuming pure ice and using the topographic profile of the north deposits measured by MOLA. She found that rather than allowing ice to flow below the trough system, the troughs separate the cap into distinct units. In this model, there is no flow between the major troughs. This is due to the fact that ice exposed in the pole-facing slopes of the troughs will either not flow at all or flow slowly towards the pole. Modelling by Greve and Mahajan (2005) indicates that, while many uncertainties associated with ice rheology and the dust content of the NPLD only allow the prediction of ice flow velocities within several orders of magnitude, probable present values are ~ 0.1 – 1 mm/yr; while work by Hvidberg and Fishbaugh (2006) imply that flow rates are small compared to mass balance rates and therefore the upper visible layer stratigraphy should not be significant affected by flow. Topographic data show slopes along the edge of the NPLD and in the troughs that are too steep to have formed from flow (Zuber et al. 1998). Zuber et al. (1998) conclude that the NPLD are flowing and ablating back to maintain a steady-state shape. Recent modeling of ice cap flow indicates that troughs within a pure water deposit would be expected to close on timescales of 10^5 to 10^6 years (Hvidberg 2003) while troughs in a deposit containing 25% dust by volume would close in 5 Myr under current obliquity conditions and in 1-2 Myrs at 35° obliquities (Pathare and Paige 2005); this may imply that other forces such as sublimation or erosion by katabatic winds are actively keeping the troughs open.

The upper 300 m of layered deposits appears to be continuous and undeformed around the NPLD (Milkovich and Head 2005, Milkovich et al. 2006); this may imply that the upper sequence of layers has not experienced stress conditions required for brittle fracture but instead flowed without deformation. Alternatively, the upper sequence of layers has not experienced flow at all. Three dimensional measurements of layer orientation (dip and strike) at various locations and elevations within the NPLD show variations from the dome-like configuration expected from a static deposit in which the troughs are recent formation cutting into pre-existing layers. This may indicate that the troughs have influenced layer formation and evolution, either through their presence at the time of layer accumulation, the deformation of layers near the surface as the troughs flow closed, or a combination of the two (Milkovich et al. 2006).

An alternate explanation for the observed features is that these layers contain crossbedding formed during primary deposition. Typical crossbedding morphology involves multiple inclined layers stacked within a layer bed; at the resolution of the MOC images, the layers in question do not appear to be made up of multiple layers. Therefore, we conclude that crossbedding is not the most plausible explanation for these features. It is possible for brittle deformation to occur without flow; for example, subsidence or tectonics below the polar deposits can also cause brittle fracturing within the NPLD. In light of the lack of knowledge concerning the recent tectonics of the plains underlying the polar deposits, we cannot determine the influence of sub-ice tectonics on the internal structure of the NPLD and interpret fault-like features as consistent with deformation.

It is important to determine whether these features are consistent with compression or extension. The deformed layer in Figure 14a in particular appears to contain several segments that have not quite broken apart but are connected and may be folded. This is similar to layer deformation in a compressive stress regime where the layer is folded to such an extreme that portions of the folds undergo faulting and low-angle overthrusting. Therefore, we interpret this layer as a compressive feature. The presence of this layer combined with the probable faulted layers in Figures 17 and 18 indicates that compressive forces were at one time present in these troughs.

The presence of features consistent with deformation such as faults in the layered deposits is evidence for flow of the NPLD at some point in their history. The scarcity of such layers may indicate that most of the layers undergo ductile flow and therefore do not form features such as boudinage or reverse thrusts and folds. Alternatively, lack of common flow features may indicate that ice flow is an infrequent occurrence in the history of the NPLD. The layers identified as having features consistent with brittle deformation are located in troughs near the edge of the NPLD; this indicates that the layers near the deposit margin have experienced some compressive shear stress. The orientation of these layers is consistent with the upper portion of the NPLD moving over the lower portion. Such behavior is consistent with our understanding of ice flow in terrestrial ice sheets and glaciers.

Tanaka (2005) identified potential deformation features in the area of ~ 82°N, 73° E which he attributed to the presence of a nearby crater. Our additional identification of features in a more widespread area of the NPLD may indicate that the features identified by Tanaka are in fact due to flow of the NPLD.

Unconformities

Studies of orbital variations and in the Amazonian period of Mars and their influence on regions of ice stability indicate that the NPLD have likely experienced significant periods of net erosion (e.g., Jakosky et al. 1993; Laskar et al. 2004). Such erosion may be recorded as unconformities in the NPLD; thus, any unconformities found in the NPLD may provide an important link to the climate history of the planet. However, the NPLD is remarkable for the long distances

(hundreds of kilometers) over which layer sequences (several hundred meters thick) may be traced (e.g., Malin and Edgett 2001; Milkovich and Head 2005; Milkovich et al. 2006). Disconformities may indicate a local interruption in NPLD accumulation, perhaps due to the influence of latitude and albedo feedback on layer formation (Kreslavsky and Head, 2006), while angular unconformities would imply a major erosional event in polar history.

Tanaka (2005) identified unconformities around the NPLD with a majority found on the opposite side of the deposits from Olympia Planita; Tanaka (2005) did not discuss these unconformities in great detail. The two examples shown in Tanaka (2005) appear to be to be disconformities.

The cluster of potential angular unconformities we have identified, if real, indicate that this region of the NPLD experienced a period of extensive erosion at some point in polar history followed by a period of net deposition. Their concentration in the 0° lobe of the NPLD may imply that this region experienced a more extreme period of erosion than the opposite portion of the NPLD, where such striking features have not yet been observed (Tanaka 2005). The angular unconformities are observed at the lowest latitudes of the NPLD; this may explain the higher erosion rates. Any angular unconformities recorded at equivalent latitudes on the opposite side of the NPLD (supposing the NPLD once extended to these latitudes) could have been erased. This could be due to retreat of one side of the NPLD as obliquity changed, as proposed by Fishbaugh and Head (2000) to account for characteristics of the circumpolar features. In addition, a majority of the candidate angular unconformities appear to be below the upper stratigraphic zones identified with Fourier analysis in the NPLD by Milkovich and Head (2005) and Milkovich et al. (2006) which are proposed to record the past approximately 2.5 Ma. This implies that the angular unconformities were formed prior to the recent low obliquity regime, and may correspond to an earlier, high-obliquity event. However, further examination of these features with improved topographic control is necessary before definite conclusions are drawn.

Exploration goals and strategy for the NPLD

Clifford et al. (2000) outlines outstanding issues to be addressed in future Mars polar spacecraft exploration and needed capabilities of those spacecraft. They highlight the need for in situ measurements of the polar deposits through surface-based platforms in order to examine the internal properties of the NPLD and provide ground truth for orbital measurements. One such surface platform for exploration is a rover; any rover mission to the north polar deposits will traverse several scarps within the layered deposits to examine the structure, composition, and chronology of the layers (Clifford et al. 2000). Our analysis of high-resolution images of the layered surfaces reveals that a polar rover would need to be capable of negotiating rough, knobby, and pitted surfaces. These surfaces may be the result of surface-atmosphere interactions and thus the composition and

structure of the underlying layers may be different than those of the immediate surface. Therefore, in order to correctly analyze the properties of the layers any rover must also have the ability to access the subsurface material through a drill, scoop, or thermal probe. An alternative exploration platform is a lander; such a mission could trade lateral mobility for more detailed analysis of one location. A lander should be able to study the subsurface material to greater depth and detail; a drill or thermal probe would be required. In order to search for clathrate deposits, an investigation of the subsurface must be capable of accessing depths of at least 1.5 m.

A review of the physical characteristics of terrestrial ice sheets highlights several fundamental physical and compositional properties of polar materials that are important for reaching a more detailed understanding of the formation, modification, and rheological behavior of the martian deposits. These include: the grain size of the ice in each layer which will inform us on the temperature conditions at the time of ice formation and what subsequent modification the layer has experienced at depth; the relative proportions of water ice, CO_2 clathrate hydrate, and dust; the grain morphology of the dust component; and the presence of tephra that will aid in chronostratigraphy. A polar surface mission should be capable of making measurements of these characteristics.

Further analysis of the NPLD using current spacecraft instrumentation as MGS, Mars Odyssey, and Mars Express continue their extended missions and Mars Reconnaissance Orbiter (MRO) begins data collection will undoubtedly be fruitful. Additional high-resolution MOC, THEMIS, and HRSC super-resolution channel images will allow for the continuing search for unconformities and deformational features within the NPLD. Stereo data provided by repeated images of the same locations by these cameras would provide topographic information to help determine if the features described here are indeed examples of deformation or unconformities, or are actually produced by regular layers exposed on unusual topography. More observations of layer surfaces at MOC and HiRISE resolutions would allow us to look for trends in layer texture with distance from the pole or with longitude. Furthermore, HiRISE images will allow us to test many of the interpretations in this paper by improving the morphological characterization of layer textures; for example, is the honeycomb network characteristic of ablation hollows clearly visible at higher resolutions? In addition, radar sounding by MARSIS and SHARAD, the Shallow Subsurface RADar onboard MRO will aid in constraining the dust content of the NPLD and provide further information on the internal layering within the deposits.

Conclusions

An examination of layer surface characteristics implies that surface textures may be influenced by physical properties of the individual layers; the characteristics of the individual layers themselves vary in response to climate change.

Surface texture may thus be influenced by recent climate change, in particular by cyclic variations in dust content. Knobby layers may be erosion-resistant layers due to low dust content or to ice grain size variations, while pitted layers are erosion-weak layers due to high dust content or to ice grain size variations. Laminated layers may be packets of alternating weak and strong layers due to changing dust content and/or ice grain size variations. Rough layers are likely to be the result of surface erosion processes such as ablation hollows. The marker bed may be an ice-rich layer representing a period where a high concentration of water was moved to the polar regions, such as outgassing from an impact crater or as part of a climate shift. Woven or imbricated textures may represent a laminated packet of layers that has undergone flow and deformation. A simple model of increasing dust content with increasing insolation during deposition may be able to explain the sequence of surface textures within the layer stratigraphy.

Other results of our analysis of polar images include evidence for layer deformation in the form of reverse faults is found in regions consistent with high stress regime associated with flow, and candidate unconformities that may record a period of extreme NPLD instability and erosion. An impact crater identified in an image centered at 83.0°N, 94.5°E displays some evidence of degradation and may have undergone burial and exhumation.

In order to further characterize the NPLD and understand their formation and modification, future surface missions to the polar regions should be prepared to measure physical properties such as grain size, composition, and respective proportions of ice and dust components, identify tephra layers, and possess the capability to access the immediate subsurface of the deposits. In addition, such a mission needs to analyze the NPLD across multiple layers and locations in order to examine the full diversity of these deposits.

Directory of supporting data

root directory
    milkovich_mars_2006_0003.pdf this file
    Fig. 3 figure3.png full-resolution figure
    Fig. 4 figure4.png full-resolution figure
    Fig. 5 figure5.png full-resolution figure
    Fig. 6 figure6.png full-resolution figure
    Fig. 7 figure7.png full-resolution figure
    Fig. 8 figure8.png full-resolution figure
    Fig. 9 figure9.png full-resolution figure
    Fig. 10 figure10.png full-resolution figure
    Fig. 11 figure11.png full-resolution figure
    Fig. 12 figure12.png full-resolution figure
    Fig. 13a figure13a.png full-resolution figure
    Fig. 13b figure13b.png full-resolution figure
    Fig. 14 figure14.png full-resolution figure
    Fig. 15 figure15.png full-resolution figure
    Fig. 16 figure16.png full-resolution figure
    Fig. 17 figure17.png full-resolution figure
    Fig. 18 figure18.png full-resolution figure
    Fig. 19 figure19.png full-resolution figure
    Fig. 20 figure20.png full-resolution figure

    Fig. 21 figure21.png full-resolution figure
    Fig. 22 figure22.png full-resolution figure
    Fig. 24 figure24.png full-resolution figure
    Fig. 25 figure25.png full-resolution figure
    Fig. 27 figure27.png full-resolution figure
    Table 2 table2.txt images used in deformation analysis

Acknowledgments

References

Alley, R. B., J. H. Perepezko and C. R. Bently (1986) "Grain growth in polar ice, II. Application" Journal of Glaciology, 32, 425-433.

Bennett, M. R. and M. F. Glasser (1996) Glacial Geology: Ice Sheets and Landforms, Wiley, Chichester.

Berman, D. C. and W. K. Hartmann (2002) "Recent fluvial, volcanic, and tectonic activity on the Cerberus Plains of Mars" Icarus, 159, 1-17, doi:10.1006/icar.2002.6920.

Betterton, M. D. (2001) "Theory of formation of structure in fnowfields: Penitentes, suncups, and dirt cones" Physical Review E, 63, 056129, doi:10.1103/PhysRevE.63.056129.

Blasius, K. R., J. A. Cutts and A. D. Howard (1982) "Topography and stratigraphy of Martian polar layered deposits" Icarus, 50, 140-160, doi:10.1016/0019-1035(82)90122-1.

Bory, A. J.-M., P. E. Biscaye and J. P. Steffensen (2003) "Regional variability of ice core dust composition and provenance in Greenland" Geochemistry Geophysics Geosystems, 4, doi:10.1029/2003GC000627.

Britt, D. T., D. C. Boice, B. J. Buratti, H. Campins and R. M. Nelson (2004) "The morphology and surface processes of Comet 19/P Borrelly" Icarus, 167, 45-53, doi:10.1016/j.icarus.2003.09.004.

Byrne, S. and B. C. Murray (2002) "North polar stratigraphy and the paleo-erg of Mars" Journal of Geophysical Research, 107, doi:10.1029/2001JE001615.

Clark, B. R. and R. P. Mullin (1976) "Martian glaciation and flow of solid CO_2" Icarus, 27, 215-228.

Clifford, S. M. (1987) "Polar basal melting on Mars" Journal of Geophysical Research, 92, 9135-9152.

Clifford, S. M. et al. (2000) "The state and future of Mars polar science and exploration" Icarus, 144, 210-242, doi:10.1006/icar.1999.6290.

Colbeck, S. C. (1997) "A review of sintering in seasonal snow" (edited by CCREL) U. S. Army Cold Regions Research and Engineering Laboratory, Report 97-10.

Cutts, J. A. (1973) "Nature and origin of layered deposits of the Martian polar regions" Journal of Geophysical Research, 78, 4231-4249.

Cutts, J. A. and B. H. Lewis (1982) "Models of climate cycles recorded in Martian polar layered deposits" Icarus, 50, 216-244.

Dunbar, N. W., G. A. Zelinski and D. T. Voisins (2003) "Tephra layers in the Siple Dome and Taylor Dome ice cores, Antarctica: sources and correlations" Journal of Geophysical Research, 108, doi:10.1029/2002JB002056.

Durham, W. B. et al. (1992) "Effects of dispersed

particulates on the rheology of water ice at planetary conditions" Journal of Geophysical Research, 97, 20,883-20,897.

Durham, W. B. et al. (1997) "Creep of water ices at planetary conditions: a compilation" Journal of Geophysical Research, 102, 16,293-16,302, doi:10.1029/97JE00916.

Edgett, K. S. et al. (2003) "Mars landscape evolution: influence of stratigraphy on geomorphology in the north polar region" Geomorphology, 52, 289-297.

Fishbaugh, K. and J. W. Head (2000) "North polar region of Mars: Topography of circumpolar deposits from Mars Orbiter Laser Altimeter (MOLA) data and evidence for asymmetric retreat of the polar cap" Journal of Geophysical Research, 105, 22,455-22,486, doi:10.1029/1999JE001230.

Fishbaugh, K. and J. W. Head (2005) "Origin and characteristics of the Mars north polar basal unit and its role in the geologic history of the region" Icarus, 174, 444-474, doi:10.1016/j.icarus.2004.06.021.

Fishbaugh, K. E.. and C. S. Hvidberg (2006) "Martian north polar layered deposits: stratigraphy and relative accumulation rate patterns" Lunar and Planetary Science XXXVII, Abstract No. 1647, Lunar and Planetary Institute, Houston.

Fisher, D. A. (1993) "If martian ice caps flow: ablation mechanisms and appearance" Icarus, 105, 501-511, doi:10.1006/icar.1993.1144.

Fisher, D. A. (2000) "Internal layers in an "accublation" ice cap: A test for flow" Icarus, 144, 289-294, doi:10.1006/icar.1999.6293.

Fisher, D. A., D. P. Winebrenner and H. Stern (2002) "Lineations on the "white" accumulation areas of the residual northern ice cap of Mars: Their relation to the "accublation" and ice flow hypothesis" Icarus, 159, 39-52, doi:10.1006/icar.2002.6877.

Garvin, J. B., S. E. H. Sakimoto, J. J. Frawley, C. C. Schnetzler and H. M. Wright (2000) "Topographic evidence for geologically recent near-polar volcanism on Mars" Icarus, 145, 648-652, doi:10.1006/icar.2000.6409.

Goldsby, D. L. and D. L. Kohlstedt (2001) "Superplastic deformation of ice: experimental observations" Journal of Geophysical Research, 106, 11,017-11,030, doi:10.1029/2000JB900336.

Greve, R., V. Klemann and D. Wolf (2003) "Ice flow and isostasy of the north polar cap of Mars" Planetary and Space Science, 51, 193-204.

Greve, R. and R. A. Mahajan (2005) "Influence of ice rheology and dust content on the dynamics of the north-polar cap of Mars" Icarus, 174, 475-485, doi:10.1016/j.icarus.2004.07.031.

Haberle, R. M., J. R. Murphy and J. Schaeffer (2003) "Orbital change experiments with a Mars general circulation model" Icarus, 161, 66-89, doi:10.1016/S0019-1035(02)00017-9.

Haflidason, H., J. Eiriksson and S. von Kreveld (2000) "The tephrochronology of Iceland and the North Atlantic region during the Middle and Late Quaternary: a review" Journal of Quaternary Science, 15, 3-22.

Hambrey, M. J. and A. G. Milnes (1975) "Boudinage in glacier ice - some examples" Journal of Glaciology, 14, 383-393.

Hartmann, W. K. and D. C. Berman (2000) "Elysium Planitia lava flows: crater count chronology and geological implications" Journal of Geophysical Research, 105, 15,011-15,025, doi:10.1029/1999JE001189.

Hayes, J. D., et al. (1976) "Variations in the Earth's orbit: pacemaker of the ice ages" Science, 194, 1121-1132.

Head, J. W., J. F. Mustard, M. A. Kreslavsky, R. E. Milliken and D. R. Marchant (2003) "Recent ice ages on Mars" Nature, 426, 797-802.

Head, J. W. and D. R. Marchant (2003) "Cold-based mountain glaciers on Mars: Western Arsia Mons" Geology, 31, 641-644.

Hecht, M. H. (2002) "Metastability of liquid water on Mars" Icarus, 156, 373-386, doi:10.1006/icar.2001.6794.

Herkenhoff, K. E. and B. C. Murray (1990) "Color and albedo of the south polar layered deposits on Mars" Journal of Geophysical Research, 95, 1343-1358.

Herkenhoff, K. E. and J. J. Plaut (2000) "Surface ages and resurfacing rates of the polar layered deposits on Mars" Icarus, 144, 243-253, doi:10.1006/icar.1999.6287.

Herkenhoff, K. E. and A. R. Vasavada (1999) "Dark material in the polar layered deposits and dunes on Mars" Journal of Geophysical Research, 104, 16,487-16,500, doi:10.1029/1998JE000589.

Herzfeld, U. C. et al. (2003) "Morphogenesis of typical winter and summer snow surface patterns in a continental alpine environment" Hydrological Process, 17, 619-649.

Hoffman, N. (2000) "White Mars: A new model for Mars' surface and atmosphere based on CO_2" Icarus, 146, 326-342, doi:10.1006/icar.2000.6398.

Hofstadter, M. D. and B. C. Murray (1990) "Ice sublimation and rheology: implications for the Martian polar layered deposits" Icarus, 84, 352-361, doi:10.1016/0019-1035(90)90043-9.

Howard, A. D., J. A. Cutts and K. R. Blasius (1982) "Stratigraphic relationships within Martian polar cap deposits" Icarus, 50, 161-215, doi:10.1016/0019-1035(82)90123-3.

Howard, A. D (2000) "The role of eolian processes in forming surface features of the martian polar layered deposits" Icarus, 144, 267-288, doi:10.1006/icar.1999.6305.

Hvidberg, C. S. (2003) "Relationship between topography and flow in the north polar cap on Mars" in Annals of Glaciology, Vol. 37, pp. 363-369.

Hvidberg, C. S. and K. E. Fishbaugh (2006) "Recent flow rates of the martian north polar layered deposits" Lunar and Planetary Science XXXVII, Abstract No. 2053, Lunar and Planetary Institute, Houston.

Imbrie, J. (1982) "Astronomical theory of the Pleistocene ice ages: a brief historical review" Icarus, 50, 408-422, doi:10.1016/0019-1035(82)90132-4.

Jakosky, B. M., B. G. Henderson and M. T. Mellon (1993) "The Mars water cycle at other epochs - recent history of the polar caps and layered terrain" Icarus, 102, 286-297, doi:10.1006/icar.1993.1049.

Jakosky, B. M., B. G. Henderson and M. T. Mellon (1995) "Chaotic obliquity and the nature of the martian climate" Journal of Geophysical Research, 100, 1579-1584.

Kang, S. et al. (2003) "Dust records from three ice cores: relationships to spring atmospheric circulation over the Northern Hemisphere" Atmospheric Environment, 37, 4823-4835.

Kargel, J. S. and J. I. Lunine (1998) "Clathrate hydrates on Earth and in the solar system" in Solar System Ices (B. Schmidt et al. editors) 97-117, Kluwer Academic Publishers, Netherlands.

Kieffer, H. H., T. Z. Martin, S. C. Chase Jr, E. D. Miner and F. D. Palluconi (1976) "Martian north pole summer temperatures: dirty water ice" Science, 194, 1341-1344.

Kieffer, H., H. (1990) "H_2O grain size and the amount of dust in Mars' residual north polar cap" Journal of Geophysical Research, 95, 1481-1493.

Kreslavsky, M. A. and J. W. Head (2002) "Conditions and principal time scales for basal melting of martian polar caps" Lunar and Planetary Science XXXIII, Abstract No. 1779, Lunar and Planetary Institute, Houston.

Kreslavsky, M. A. and J. W. Head (2006) "Evolution and inner structure of the polar layered deposits on Mars: a simple deposition/ablation balance model" Lunar and Planetary Science XXXVII, Abstract No. 2058, Lunar and Planetary Institute, Houston.

Kolb, E. J. and K. L. Tanaka (2001) "Geologic history of the polar regions of Mars based on Mars global surveyor data - II. Amazonian period" Icarus, 154, 22-39, doi:10.1006/icar.2001.6676.

Koutnik, M., S. Byrne and B. Murray (2002) "South polar layered deposits of Mars: The cratering record" Journal of Geophysical Research, 107, doi:10.1029/2001JE001805.

Langevin, Y., F. Poulet, J-P Bibring, B. Schmitt, S. Doutér and B. Gondet (2005) "Summer evolution of the north polar cap of Mars as observed by OMEGA/Mars Express" Science 307, 1581-1584, doi:10.1126/science.1109438.

Langevin, Y., F. Poulet, J-P Bibring and B. Gondet (2005) "Sulfates in the north polar region of Mars detected by OMEGA/Mars Express" Science 307, 1584-1586, doi:10.1126/science.1109091.

Laskar, J., A. C. M. Correia, M. Gastineau, F. Joutel, B. Levrard and P. Robutel (2004) "Long term evolution and chaotic diffusion of the insolation quantities of Mars" Icarus, 170, 343-364, doi:10.1016/j.icarus.2004.04.005.

Laskar, J., B. Levrard and J. F. Mustard (2002) "Orbital forcing of the martian polar layered deposits" Nature, 419, 375-377.

Levrard, B., F. Forget, F. Montmessin and J. Laskar (2004) "Recent ice-rich deposits formed at high latitudes on Mars by sublimation of unstable equatorial ice during low obliquity" Nature, 431, 1072-1075, doi:10.1038/nature03055

Lorenz, R. D. (2000) "Microtektites on Mars: Volume and texture of distal impact ejecta deposits" Icarus, 144, 353-366, doi:10.1006/icar.1999.6303.

Malin, M. C. and K. S. Edgett (2001) "Mars Global Surveyor Mars Orbiter Camera: Interplanetary cruise through primary mission" Journal of Geophysical Research, 106, 23,429-423,570, doi:10.1029/2000JE001455.

Mangold, N., P. Allemand, P. Duval, Y Geraud and P. Thomas (2002) "Experimental and theoretical deformation of ice-rock mixtures: Implications on rheology and ice content of Martian permafrost" Planetary and Space Science, 50, 385-401.

Mangold, N., F. Costard and F. Forget (2003) "Debris flows over sand dunes on Mars: Evidence for liquid water" Journal of Geophysical Research, 108, doi:10.1029/2002JE001958.

Márquez, Á., C. Fernández, F. Anguita, A. Farelo, J. Anguita and M-Á de La Casa (2004) "New evidence for a volcanically, tectonically, and climatically active Mars" Icarus, 172, 573-587, doi:10.1016/j.icarus.2004.07.015.

Mellon, M. T. (1996) "Limits on the CO_2 content of the Martian polar deposits" Icarus, 124, 268-279. doi:10.1006/icar.1996.0203.

Mellon, M. T., and B. M. Jakosky (1995) "The distribution and behavior of martian ground ice during past and present epochs" Journal of Geophysical Research, 100, 11,781-11,799, doi:10.1029/95JE01027.

Milkovich, S. M. and J. W. Head (2005) "North polar cap of Mars: Polar layered deposit characterization and identification of a fundamental climate signal"

Journal of Geophysical Research, 110, doi:10.1029/2004JE002349.

Milkovich, S. M., J. W. Head and G. Neukum (2006) "Stratigraphic analysis of the north polar cap of Mars: Recent climate history" Planetary and Space Science, in press.

Miller, S. L. and W. D. Smythe (1970) "Carbon dioxide clathrate in the martian ice cap" Science, 170, 531-533.

Mischna, M. A., M. I. Richardson, R. J. Wilson and D. J. McCleese (2003) "On the orbital forcing of Martian water and CO_2 cycles: A general circulation model study with simplified volatile schemes" Journal of Geophysical Research, 108, doi:10.1029/2003JE002051.

Nolin, A. W. (1998) "Mapping the Martian polar ice caps: Applications of terrestrial optical remote sensing methods" Journal of Geophysical Research, 103, 25,851-25,864, doi:10.1029/98JE02082.

Nolin, A. W. and J. Dozier (2000) "A hyperspectral method for remotely sensing the grain size of snow" Remote Sensing of Environment, 74, 207-216.

Nye, J. F. (2000) "A flow model for the polar caps of Mars" Journal of Glaciology, 46, 438-444.

Paige, D. A. (1992) "The thermal stability of near-surface ground ice on Mars" Nature, 356, 1992, 43-45, doi:10.1038/356043a0.

Paige, D. A. et al. (1994) "Thermal and albedo mapping of the polar regions of Mars using Viking thermal mapper observations: 1. North polar region" Journal Of Geophysical Research, 99, 25,959-925,991.

Paige, D. A. and K. D. Keegan (1994) "Thermal and albedo mapping of the polar regions of Mars using Viking thermal mapper observations: 2. South polar region" Journal of Geophysical Research, 99, 25,993-26,013.

Palais, J. M., J. E. Bachman and K. D. Keegan (1988) "Magmatic and phreatomagmatic volcanic activity at Mt Takahe, West Antarctica, based on tephra layers in the Byrd ice core and field observations at Mt. Takahe" Journal of Volcanology and Geothermal Research, 35, 295-317.

Paterson, W. S. B. (1994) The Physics of Glaciers, Pergamon, New York.

Pathare, A. V. and D. A. Paige (2005) "The effects of martian orbital variations upon the sublimation and relaxation of north polar troughs and scarps" Icarus, 174, 419-443, doi:10.1016/j.icarus.2004.10.030.

Petit, J. R., J. Jouzel, L. Mounier, Y. S. Korotkevich and V. I. Kotliakov (1990) "Palaeoclimatological and chronological implications of the Vostok core dust record" Nature, 343, 56-58.

Picardi, G. et al. (2005) "Radar soundings of the subsurface of Mars" Science, 310, 1925-1928, doi:10.1126/science.1122165.

Pollard, A. M. et al. (2003) "Chemical alteration of tephra in the depositional environment: theoretical stability modeling" Journal of Quaternary Science, 18, 385-394.

Post, A. and E. R. LaChapelle (1971) Glacier Ice, University of Washington, Seattle and London.

Ramsay, J. G. (1967) Folding and Fracturing of Rocks, McGraw Hill, New York.

Rhodes, J. J. et al. (1987) "Mode of formation of "ablation hollows" controlled by dirt content of snow" Journal of Glaciology, 33, 135-139.

Ross, R. G. and J. S. Kargel (1998) "Thermal conductivity of solar system ices, with special reference to martian polar caps" in Solar System Ices (B. Schmidt et al. editors) 33-62, Kluwer Academic Publishers, the Netherlands.

44

Schultz, P. H. and J. F. Mustard (2001) "Impact glass strewnfields on Mars" Lunar and Planetary Science XXXII, Abstract No. 1668, Lunar and Planetary Institute, Houston.

Settle, M. (1979) "Formation and deposition of volcanic sulfate aerosols on Mars" Journal of Geophysical Research, 84, 8343-8354.

Shean, D. E., J. W. Head and D. R. Marchant (2005) "Origin and evolution of a cold-based tropical mountain glacier on Mars: The Pavonis Mons fan-shaped deposit" Journal of Geophysical Research, 110, doi:10.1029/2004JE002360.

Soderblom, L. A., M. C. Malin, J. A. Cutts and B. C. Murray (1973) "Mariner 9 observations of the surface of Mars in the north polar regions" Journal of Geophysical Research, 78, 4197-4310.

Squyres, S. W. (1979) "The evolution of dust deposits in the martian north polar region" Icarus, 40, 244-261.

Tanaka, K. L. (2005) "Geology and insolation-driven climatic history of Amazonian north polar materials on Mars" Nature 437, 991-994 doi:10.1038/nature04065.

Thomas, P. et al. (1992) "Polar deposits of Mars" in Mars, edited by H. H. Kieffer, et al., pp. 767-795, University of Arizona Press, Tucson, AZ.

Thomas, P. and C. Weitz (1989) "Sand dune materials and polar layered deposits on Mars" Icarus, 81, 185-215, doi:10.1016/0019-1035(89)90133-4.

Thomas, P. C., M. C. Malin, K. S. Edgett, M. H. Carr, W. K. Hartmann, A. P. Ingersoll, P. B. James, L. A. Soderblom, J. Veverka and R. Sullivan (2000) "North-south geological differences between the residual polar caps on Mars" Nature, 404, 161-164.

Thorsteinsson, T., J. Kipfstuhl, H. Eicken, S. J. Johnsen and K. Fuhrer (1995) "Crystal size variations in Eemian-age ice from the GRIP ice core, Central Greenland" Earth and Planetary Science Letters, 131, 381-394, doi:10.1016/0012-821X(95)00031-7.

Thorsteinsson, T., J. Kipfstuhl and H. Miller (1997) "Textures and fabrics in the GRIP ice core" Journal of Geophysical Research, 102, 26,583-26,599, doi:10.1029/97JC00161.

Ward, W. R. (1992) "Long-term orbital and spin dynamics of Mars" in Mars (H. H. Kieffer et al. editors) 298-320, University of Arizona Press, Tucson, AZ.

Wilson, L. and J. W. Head (1994) "Mars: review and analysis of volcanic eruption theory and relationships to observed landforms" Reviews of Geophysics, 32, 221-263.

Wilson, L. and J. W. Head (2005) "The nature and dispersal of pyroclastic eruptive products on Mars: relation to the characteristics of surface deposits and geologic units" Vernadsky/Brown Microsymposium, 42, Abstract.

Workman, F. B. and W. H. Workman (1909) Peaks and Glaciers of Nun Kun, Charles Scribner's Sons, New York.

Wrobel, K. E. and P. H. Schultz (2004) "Effect of planetary rotation on distal tektite deposition on Mars" Journal of Geophysical Research, 109, doi:10.1029/2004JE002250.

Zhou, X., S. Li and K. Stamnes (2003) "Effects of vertical inhomogeneity on snow spectral albedo and its implication for optical remote sensing of snow" Journal of Geophysical Research, 108, doi:10.1029/2003JD003859.

Zielinski, G. A., and M. S. Germani (1998) "New ice-core evidence challenges the 1620s BC age for the Santorini (Minoan) eruption" Journal of Archaeological Science, 25, 279-289.

Zielinski, G. A. et al. (1997) "Volcanic aerosol records and tephrochronology of the Summit, Greenland ice core" Journal of Geophysical Research, 26,625-26,640, doi:10.1029/96JC03547.

Zuber, M. T., et al. (1998) "Observations of the north polar region of Mars from the Mars Orbiter Laser Altimeter" Science, 282, 2053-2060.